Received: 18 June 2020 | Accepted: 23 November 2020

DOI: 10.1111/bpa.12921

Brain Pathology

RESEARCH ARTICLE

The presence of TIM-3 positive cells in WHO grade III and IV astrocytic gliomas correlates with isocitrate dehydrogenase mutation status

Mia D. Sørensen[1,2] | **Ole Nielsen**[1] | **Guido Reifenberger**[2,3,4] | **Bjarne W. Kristensen**[1,2,5,6]

[1]Department of Pathology, Odense University Hospital, Odense, Denmark

[2]Department of Clinical Research, University of Southern Denmark, Odense, Denmark

[3]Institute of Neuropathology, Heinrich Heine University, Düsseldorf, Germany

[4]German Cancer Consortium (DKT), partner site Essen/Düsseldorf, Essen, Germany

[5]Department of Pathology, Rigshospitalet, Copenhagen University Hospital, Copenhagen, Denmark

[6]Department of Clinical Medicine and Biotech Research and Innovation Center (BRIC), University of Copenhagen, Copenhagen, Denmark

Correspondence
Mia D. Sørensen, Department of Pathology, Odense University Hospital, J. B. Winsløws Vej 15, 5000, Odense C, Denmark.

Funding information
Danish Council for Independent Research, Grant/Award Number: 4183-00183

Abstract

Diffuse gliomas are aggressive brain tumors that respond poorly to immunotherapy including immune checkpoint inhibition. This resistance may arise from an immunocompromised microenvironment and deficient immune recognition of tumor cells because of low mutational burden. The most prominent genetic alterations in diffuse glioma are mutations in the isocitrate dehydrogenase (IDH) genes that generate the immunosuppressive oncometabolite D-2-hydroxyglutarate. Our objective was to explore the association between IDH mutation and presence of cells expressing the immune checkpoint proteins galectin-9 and/or T cell immunoglobulin and mucin-domain containing-3 (TIM-3). Astrocytic gliomas of World Health Organization (WHO) grades III or IV (36 IDH-mutant and 36 IDH-wild-type) from 72 patients were included in this study. A novel multiplex chromogenic immunohistochemistry panel was applied using antibodies against galectin-9, TIM-3, and the oligodendrocyte transcription factor 2 (OLIG2). Validation studies were performed using data from The Cancer Genome Atlas (TCGA) project. IDH mutation was associated with decreased levels of TIM-3$^+$ cells ($p < 0.05$). No significant association was found between galectin-9 and IDH status ($p = 0.10$). Most TIM-3$^+$ and galectin-9$^+$ cells resembled microglia/macrophages, and very few TIM-3$^+$ and/or galectin-9$^+$ cells co-expressed OLIG2. The percentage of TIM-3$^+$ T cells was generally low, however, IDH-mutant tumors contained significantly fewer TIM-3$^+$ T cells ($p < 0.01$) and had a lower interaction rate between TIM-3$^+$ T cells and galectin-9$^+$ microglia/macrophages ($p < 0.05$). TCGA data confirmed lower *TIM-3* mRNA expression in IDH-mutant compared to IDH-wild-type astrocytic gliomas ($p = 0.013$). Our results show that IDH mutation is associated with diminished levels of TIM-3$^+$ cells and fewer interactions between TIM-3$^+$ T cells and galectin-9$^+$ microglia/macrophages, suggesting reduced activity of the galectin-9/TIM-3 immune checkpoint pathway in IDH-mutant astrocytic gliomas.

KEYWORDS
galectin-9, glioma, immune checkpoint, immunohistochemistry, isocitrate dehydrogenase, microglia, multiplex, TIM-3

1 | INTRODUCTION

Somatic mutations in the genes *isocitrate dehydrogenase* (*IDH*) *1* or *2* are found in ~80% of patients with WHO grade II–III diffuse gliomas (1–4). These mutations most frequently occur at codon R132 in *IDH1* or at the homologous residues R172 or R140 in *IDH2*, and are considered early events in gliomagenesis (5–7). IDH mutations were first reported in gliomas in 2008 (2) and have since been discovered in other cancers including acute leukemia (8, 9), angioimmunoblastic T cell lymphoma (10), chondrosarcoma (11, 12), melanoma (13), cholangiocarcinoma (14, 15), and prostate cancer (16). IDH1 is located in the cytoplasm and peroxisomes, whereas IDH2 is found in the mitochondrial matrix, however, both enzymes play important roles in several cellular functions, including glucose sensing, glutamine metabolism, lipogenesis, and regulation of cellular redox balance, especially in the human brain (6, 17). IDH active site mutations result in a neomorphic enzymatic activity generating the oncometabolite D-2-hydroxyglutarate instead of α-ketoglutarate, with concomitant consumption of NADPH to $NADP^+$ (5–7). In IDH-mutant gliomas, D-2-hydroxyglutarate accumulates intra- and extracellularly up to concentrations that are 100-fold higher than in IDH-wildtype gliomas (5, 18, 19). D-2-hydroxyglutarate modifies the cellular energetics and epigenetics, including promotion of a DNA hypermethylation phenotype (5–7, 20–23).

Increasing data indicate that IDH mutation and D-2-hydroxyglutarate may modulate the tumor microenvironment and its nonneoplastic cells. Reportedly, IDH-mutant gliomas show suppressed antithrombotic and anticoagulant pathways (24, 25) and have a distinct vascular gene expression signature (26) compared to IDH-wildtype tumors. In addition, mutation in the *IDH* genes has been shown to impact the glioma-associated immune landscape. Generally, the immune microenvironment in gliomas is considered "cold" (27), lymphocyte-depleted/immunological quiet (28), and immunosuppressive because of tumor extrinsic and intrinsic mechanisms (27, 29, 30). IDH mutation and the consecutive expression of the D-2-hydroxyglutarate have been reported to alter the level of immune cell infiltration (20, 28, 31–37), immune activation/response (20, 22, 31, 33, 34, 37–41), and immune checkpoint systems (32–34, 42–44), overall hampering the immunosurveillance and immune-mediated destruction enabling development of "cold" tumors.

Immune responses are tightly regulated by an immune checkpoint system that adjusts the duration and amplitude preventing autoimmunity and tissue damage. Stimulatory checkpoint pathways promote activation of T cells, while inhibitory pathways confine the threshold for T cell activation and regulate resolution of inflammation, tolerance, and homeostasis. In malignancies, the inhibitory checkpoints can be exploited by the cancer cells to escape immune surveillance. Immunotherapy targeting co-inhibitory immune checkpoints, especially cytotoxic T lymphocyte antigen 4 (CTLA-4) and programed death receptor 1 (PD-1), has proven effective in several cancers including melanoma and non-small cell lung carcinoma, with combination therapies that target two co-inhibitory receptors/pathways showing increased antitumor efficacy (45–47). Another inhibitory checkpoint system of increasing interest in cancer immunotherapy is the galectin-9 (Gal-9)/T cell immunoglobulin and mucin-domain containing-3 (TIM-3) pathway. TIM-3 is expressed by different subsets of T cells and promotes T cell tolerance when interacting with its ligands including Gal-9. Additionally, TIM-3 has been linked to T cell exhaustion and dysfunction, especially when co-expressed with PD-1 (45, 48–51). Reportedly, TIM-3 is also expressed by cancer cells and cells of the myeloid lineage including macrophages in both noncancerous and cancerous tissues, and TIM-3 has been shown to regulate immune responses in these cell types as well (48, 52–54). In glioma, Gal-9 (55–57) and TIM-3 (56, 58, 59) have been correlated to tumor aggressiveness, however, little knowledge exists about (a) the protein expression patterns of Gal-9 and TIM-3 at a cell type-specific level in glioma tissue and (b) the association between IDH mutation and expression/activation of the Gal-9/TIM-3 checkpoint system.

The aim of this study was to determine whether protein expression of the Gal-9/TIM-3 checkpoint pathway is affected by IDH mutation status in diffuse astrocytic glioma. Therefore, we investigated glioma tissue samples from a patient cohort with WHO grade III or IV astrocytic gliomas stratified according to IDH status using a novel brightfield multiplex chromogenic immunohistochemistry panel consisting of antibodies against Gal-9, TIM-3, and oligodendrocyte transcription factor 2 (OLIG2). OLIG2 was included in the panel as a glial marker that is commonly expressed in tumor cells of astrocytic gliomas (60, 61) and was used to identify the potential expression of Gal-9 and/or TIM-3 by glial tumor cells. This multiplexing approach facilitated that specific cell subpopulations including co-localization and interaction patterns could be identified within the same tissue slide.

2 | MATERIAL AND METHODS

2.1 | Patient tissue

Formalin-fixed, paraffin-embedded tissue samples from 72 adult glioma patients were used for the multiplex chromogenic immunohistochemistry part of the study. All patients underwent initial surgery between 1997 and 2017 at the Department of Neurosurgery, Odense University Hospital, Odense, Denmark, or at the Department of

Neurosurgery, Heinrich Heine University, Düsseldorf, Germany. The tumor samples were classified according to the WHO Classification 2016 (62). The 72 samples included: 23 IDH-mutant anaplastic astrocytomas, WHO grade III; 16 IDH-wildtype anaplastic astrocytomas, WHO grade III; 14 IDH-mutant glioblastomas, WHO grade IV; and 19 IDH-wildtype glioblastomas, WHO grade IV. IDH status was determined by immunohistochemistry or DNA sequencing as previously described (37, 63). The cohort has been used previously (37), and immunostaining results for CD4, CD8, and FOXP3 from the study were used for correlation analyses in the present study. For the present study, the cohort was additionally immunostained with antibodies against ionized calcium-binding adaptor molecule 1 (IBA-1) and CD204.

A tissue array containing eight to nine IDH-wild-type glioblastoma specimens was included for the double immunofluorescence part of the study to investigate the co-expression patterns of Gal-9/TIM-3, Gal-9/OLIG2, Gal-9/IBA-1, TIM-3/OLIG2, TIM-3/IBA-1, and TIM-3/CD3. In addition, four IDH1 R132H-mutant grade III–IV astrocytic gliomas were selected for double immunofluorescence stainings to examine the co-expression patterns of Gal-9/IDH1 R132H and TIM-3/IDH1 R132H.

2.2 | Multiplex chromogenic immunohistochemistry

A multiplex chromogenic immunohistochemistry panel (Figure 1) was implemented on the Discovery Ultra autostainer (Ventana Medical Systems, Tucson, AZ, USA) by sequential application of unconjugated primary antibodies with heat deactivation steps in between each sequence for elution purposes. Appropriate staining controls were performed during the panel development to check for possible cross-reactivity related to the detection systems.

Three µm sections from formalin-fixed, paraffin-embedded tissue blocks were mounted on FLEX IHC slides (Dako, Glostrup, Denmark). The tissue sections were subjected to a standard immunostaining protocol including deparaffinization, epitope retrieval in Cell Conditioning 1 buffer (CC1, #950-500, Ventana) for 32 min and blockade of endogenous peroxidase activity. Following the incubation and detection steps described in Table 1, the tissue slides were counterstained with Hematoxylin II (#790-2208, Ventana) and Bluing Reagent (#760-2037, Ventana), dehydrated and cleared. Coverslips were mounted using Pertex® Mounting Medium (#00811, Histolab Products AB, Gothenburg, Sweden). Slides were digitized using a Hamamatsu Digital Slide Scanner (Hamamatsu, Japan).

2.3 | Stereological-based cell counting

Stereological-based image analysis was performed in the Visiopharm software module Stereology (Visiopharm, Hørsholm, Denmark). Vital tumor areas were manually outlined as regions of interest, guided by representative adjacent hematoxylin-eosin stains. Normal brain tissue and areas of tumor infiltration as well as larger areas of necrosis and blood vessels were excluded Sample images were acquired using systematic uniform random sampling (meander: number of samples-based) at 20× magnification. The sampling algorithm was optimized to achieve accurate cell counting. Ultimately, the number of sample images was set at 10 images per tumor. Cell counting was done using a 2 × 2 counting frame that covered 10% of the sampled image area. Reproducibility was tested by independently performing random sampling

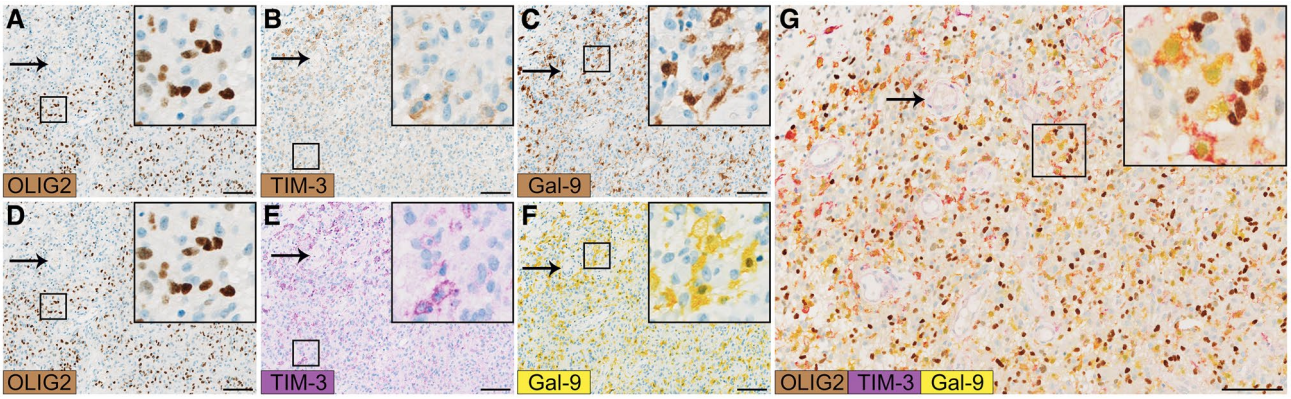

FIGURE 1 Design of the multiplex chromogenic immunohistochemistry panel. The multiplex immunohistochemistry assay was designed after implementing the antibodies by conventional DAB staining (A–C). Chromogens were then assigned for each antibody; brown for the nuclear OLIG2 (D), purple for the membranous/cytoplasmic TIM-3 (E), and yellow for the cytoplasmic Gal-9 (F). For each marker, the staining pattern of the individual DAB-stained slides was comparable to the matched single colored chromogen slide. The multiplexed staining obtained with the panel is shown in G. The use of translucent chromogens (purple and yellow) produced color changes at sites of chromogenic co-localization (red) allowing easy and reliable identification of co-expressing cells, that is, TIM-3$^+$ Gal-9$^+$ cells. No color mixing was observed between OLIG2 (brown) and TIM-3 (purple) or Gal-9 (yellow) as OLIG2 is expressed in the nuclei. *Scale bar* 100 µM

TABLE 1 Summary of technical conditions used for the multiplex chromogenic immunohistochemistry panel

	OLIG2/TIM-3/Gal-9 multiplex panel
Pretreatment	Cell Conditioning 1 (CC1, #950-500) 32 min 100°C
Inhibitor	Inhibitor CM (#760-4307) 8 min
Primary Ab #1	Anti-OLIG2 rabbit polyclonal Ab (Immuno-Biological Laboratories, #18953) 1:200, 32 min 36°C
Detection	Anti-Rabbit-HQ (#760-4815) 20 min + anti-HQ-HRP (#760-4820) 20 min
Amplification	No
Chromogen	ChromoMap DAB kit (#760-159) 4 + 8 min
Elution	Cell Conditioning 2 (CC2, #950-123) 8 min 100°C
Primary Ab #2	Anti-TIM-3 rabbit monoclonal Ab (Cell Signaling Technology, clone D5D5R) 1:25, 60 min 36°C
Detection	Anti-Rabbit-HQ (#760-4815) 16 min + anti-HQ-HRP (#760-4820) 16 min
Amplification	No
Chromogen	Purple kit (#760-229) 32 min
Elution	CC2 8 min 100°C
Primary Ab #3	Anti-Gal-9 rabbit monoclonal Ab (Cell Signaling Technology, clone D9R4A) 1:100, 48 min 36°C
Detection	Anti-Rabbit-NP (#760-4817) 12 min + anti-NP-AP (#760-4827) 12 min
Amplification	No
Chromogen	Yellow kit (#760-239) 44 min

Note: Apart from the antibodies, the slides were colored using #Ventana reagents. Prior to the development of the multiplex panel, all antibodies were implemented as conventional immunohistochemistry DAB stainings using OptiView (Ventana) as detection system and then tested with the Discovery HQ-HRP detection system (anti-Rabbit-HQ 20 min + anti-HQ-HRP 20 min) using DAB as chromogen.

Abbreviations: Ab, antibody; AP, alkaline phosphatase; HRP, horseradish peroxidase; NP, nitropyrazole.

and cell counting twice on a training set of seven glioblastomas ($r_s = 0.91$, $p < 0.001$).

Eight different cell populations were counted. Tumor cells were defined as OLIG2$^+$ cells. Tumor-associated microglia/macrophages (TAMs) were defined as OLIG2$^-$ cells with expression of Gal-9 and/or TIM-3 with microglial/macrophage-like morphology (i.e., larger cells that were ameboid, elongated, or ramified in shape with evident cytoplasm). T cells were defined as OLIG2$^-$ Gal-9$^-$ TIM-3$^+$ cells with lymphocyte morphology (i.e., smaller round-shaped cells with prominent nuclei and sparse cytoplasm). Endothelial cells were not counted. The number of cells in the following cell populations was quantified:

(i) Negative cells (OLIG2$^-$ TIM-3$^-$ Gal-9$^-$ cells)
(ii) TIM-3$^-$ and Gal-9$^-$ tumor cells (OLIG2$^+$ TIM-3$^-$ Gal-9$^-$ cells)
(iii) TIM-3$^-$ and Gal-9$^+$ tumor cells (OLIG2$^+$ TIM-3$^-$ Gal-9$^+$ cells)
(iv) TIM-3$^+$ and Gal-9$^+$ tumor cells (OLIG2$^+$ TIM-3$^+$ Gal-9$^+$ cells)
(v) Gal-9$^+$ TAMs (OLIG2$^-$ TIM-3$^-$ Gal-9$^+$ cells)
(vi) TIM-3$^+$ and Gal-9$^+$ TAMs (OLIG2$^-$ TIM-3$^+$ Gal-9$^+$ cells)
(vii) TIM-3$^+$ TAMs (OLIG2$^-$ TIM-3$^+$ Gal-9$^-$ cells with microglial/macrophage-like morphology)
(viii) TIM-3$^+$ T cells (OLIG2$^-$ TIM-3$^+$ Gal-9$^-$ cells with lymphocyte morphology)

Additionally, the number of interactions between TIM-3$^+$ T cells and Gal-9$^+$ cells was assessed. To count as an interaction, a TIM-3$^+$ T cell had to be in direct contact with a Gal-9$^+$ cell, with no other cell type residing in between the two cells. The interaction rate was estimated by dividing the interaction count with the TIM-3$^+$ T cell count. Cells fractions were calculated for the specific cell population based on the total cell count as well as on the total number of tumor cells for the tumor cell population and the total number of TAMs for the TAM cell population. All fractions were converted to percentages by multiplying by 100.

2.4 | Conventional immunohistochemistry and automated quantitative image analysis

Formalin-fixed, paraffin-embedded tissue specimens were processed as described above. The tissue sections were stained according to a standard immunostaining

protocol including deparaffinization, epitope retrieval in CC1 (Ventana) for 32 min at 100°C, and blockade of endogenous peroxidase activity. Sections were then incubated with primary antibodies against IBA-1 (cat. no. 019-19741, Wako Pure Chemical Ind., Ltd., dilution 1:2000) and CD204 (clone SRA-E5, Cosmo Bio Co. LTD, dilution 1:600) for 16 and 32 min, respectively, at 36°C. Detection was performed using the OptiView DAB IHC Detection Kit (#760-700, Ventana). The processes of counterstaining, coverslipping, and slide digitization were performed as described above. Automated digital image analysis and quantification were done in the Visiopharm APP author module as previously described (64, 65). Output variables were percentages of positive area, defined as the area of positive expression divided by the total area of interest multiplied by 100.

2.5 | Double immunofluorescence and automated quantitative image analysis

Three μm sections from a formalin-fixed, paraffin-embedded tissue microarray were mounted onto FLEX IHC slides (Dako) and stained on the DISCOVERY Ultra autostainer (Ventana) (Table S1). Following deparaffinization, epitope retrieval was performed in CC1 buffer for 32 or 48 min at 100°C, and endogenous peroxidase activity was inhibited with Inhibitor CM. Slides were then incubated with primary antibody #1 (Gal-9, TIM-3, or IDH1 R132H) followed by detection with DISCOVERY OmniMap anti-Rabbit or anti-Mouse HRP (#760-4311)/DISCOVERY Cyanine 5 Kit (#760-238) system. Next, heat denaturation was performed in Cell Conditioning 2 buffer for 8 min at 100°C followed by incubation with primary antibody #2 (OLIG2, IBA-1, CD3, Gal-9, or TIM-3). The antigen-antibody complex was detected with the DISCOVERY OmniMap anti-Rabbit HRP/DISCOVERY FAM kit (#760-243) system. Slides were coverslipped with VECTASHIELD® Mounting Media containing 4,6-diamidino-2-phenylindole (DAPI) (VWR International, Radnor, PA, USA).

Super images were generated at 1.25× magnification using brightfield settings and the Visiopharm integrated microscope and software module connected to a Leica DM 6000B microscope with Olympus DP72 camera (Olympus, Ballerup, Denmark) and a Ludl motorized stage. Sample images were obtained as described above. Images were analyzed by generating pixel- and threshold-based algorithms in the Visiopharm APP author module as described previously (65). Output variables were percentages of double-positive area, defined as the area of double-positive expression divided by the total area of respective area of interest multiplied by 100.

2.6 | TCGA patient data set analyses

The mRNA expression levels of *OLIG2*, *TIM-3* (also known as Hepatitis A virus cellular receptor 2, *HAVCR2*), and *Gal-9* (*LGALS9*) as well as *CD4*, *CD8A*, *CD8B*, *FOXP3*, allograft inflammatory factor 1 (*AIF1*, also known as IBA-1), macrophage scavenger receptor 1 (*MSR1*, also known as CD204), secreted phosphoprotein 1 (*SPP1*, also known as osteopontin), interleukin-1Bβ (*IL1B*), *IL6*, *IL18*, C–C motif chemokine ligand 2 (*CCL2*), and Toll-like receptor (*TLR*)-1, 2, and 8 were examined in data sets of WHO grade III–IV astrocytomas included in The Cancer Genome Atlas (TCGA) database using GlioVis (http://gliovis.bioinfo.cnio.es/, data exported June or October 2020) (66). mRNA data were available for 255 tumors with known IDH status and without 1p/19q codeletion (67). The 255 tumors included 42 IDH-wild-type anaplastic astrocytomas, WHO grade III; 72 IDH-mutant anaplastic astrocytomas, WHO grade III; 133 IDH-wild-type glioblastomas, WHO grade IV; and eight IDH-mutant glioblastomas, WHO grade IV. Additionally, mRNA expression levels of some of the same genes were investigated in a data set of 160 WHO grade II and III gliomas with known IDH status with or without 1p/19q codeletion (67). These 160 tumors included 65 IDH-mutant and 1p/19q-codeleted oligodendrogliomas, WHO grade II; 43 IDH-mutant and 1p/19q-codeleted anaplastic oligodendrogliomas, WHO grade III; 43 IDH-mutant (1p/19q-non-codeleted) diffuse astrocytomas, WHO grade II; and 9 IDH-wild-type (1p/19q-non-codeleted) diffuse astrocytomas, WHO grade II. Differential expression analysis was done using the TCGA Agilent-4502A glioblastoma data set (68) to explore quantitative changes in mRNA expression levels of 17,811 genes between the groups of glioblastomas with the highest (n = 122) and lowest (n = 120) mRNA expression level of TIM-3. Kyoto Encyclopedia of Genes and Genomes (KEGG) and Gene Ontology (GO) enrichment analyses were performed for the differentially regulated genes using the GlioVis explore module with the following input parameters: p-value: 0.05; q-value: 0.05; and log2 fold change (FC): 2.

2.7 | Statistical analyses

Mann–Whitney U-test or Student's unpaired t-test was used to investigate the difference in protein or mRNA expression levels between IDH-mutant and IDH-wild-type tumors. One-way ANOVA with Bonferroni's Multiple Comparison Test or Kruskal–Wallis test with Dunn's Multiple Comparison Test was used when comparing more than two groups. Correlation analyses were done using Spearman's correlation test. Statistical analyses were performed in Prism (Version 5, GraphPad Software Inc., San Diego, CA, USA). $p < 0.05$ was considered significant.

3 | RESULTS

3.1 | Cellular expression patterns of Gal-9 and TIM-3

In all tumor specimens, most Gal-9$^+$ and/or TIM-3$^+$ cells morphologically resembled microglia/macrophages (Figure 1). TIM-3 was primarily located in the membrane, while Gal-9 showed a cytoplasmic expression pattern. The expression of Gal-9 and TIM-3 by IBA-1$^+$ microglia/macrophages was confirmed using double immunofluorescence as ~80% of the Gal-9 and TIM-3 area co-expressed IBA-1, whereas only ~30% and ~20% of the IBA-1 signal co-localized with Gal-9 and TIM-3 signals, respectively (Figure 2A–D). Most TIM-3$^+$ cells co-expressed Gal-9, while many of Gal-9$^+$ cells lacked expression of TIM-3 (Figures 1 and 3), and this was validated with double immunofluorescence (Figure 2E,F). Very few TIM-3$^+$ Gal-9$^-$ cells were observed, and these cells either resembled T cells or microglia/macrophages (Figure 3). T cell expression of TIM-3 was confirmed by double immunofluorescence showing that ~10% of CD3$^+$ T cells co-expressed TIM-3 (Figure 2G,H).

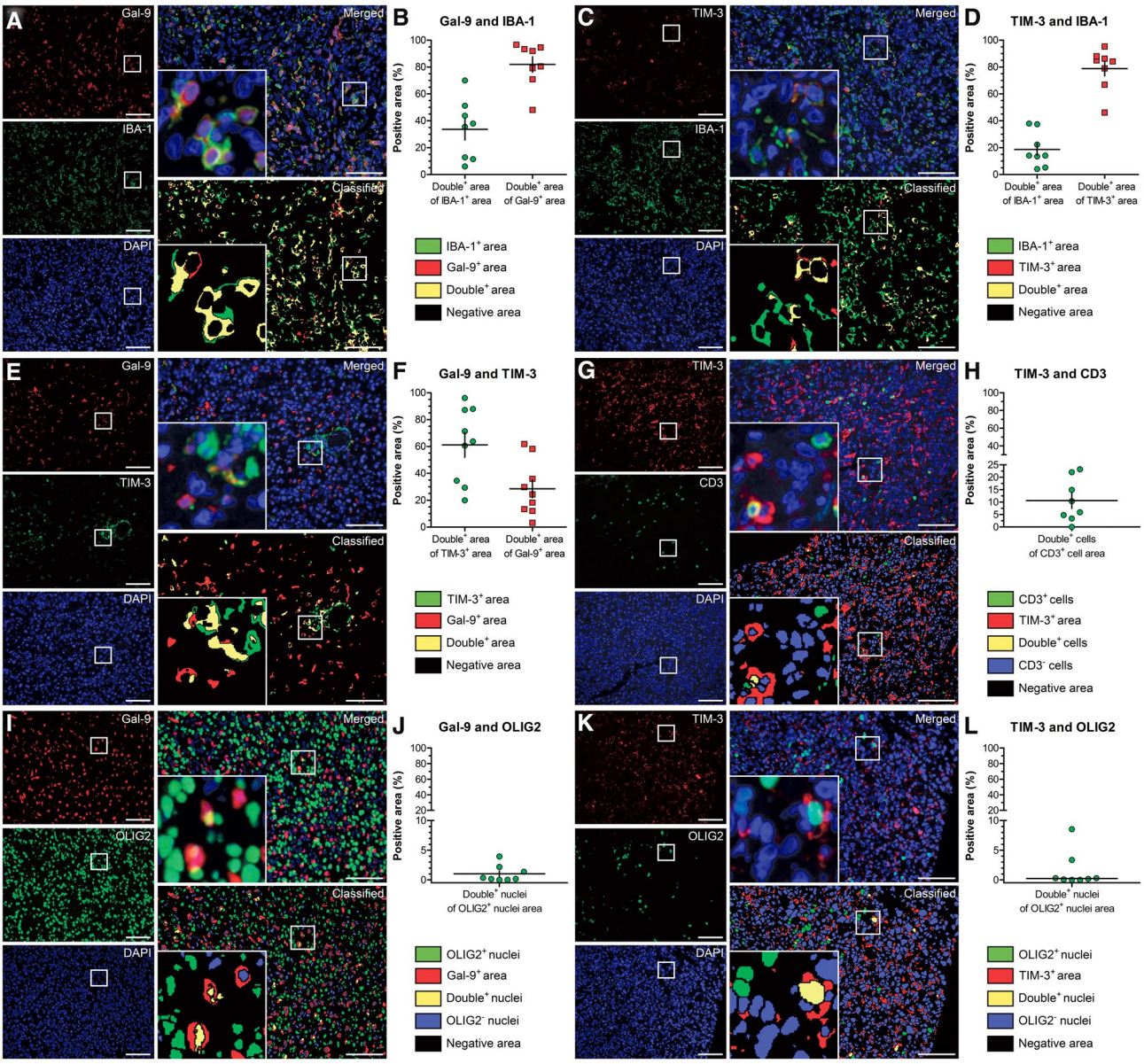

FIGURE 2 Co-expression patterns of Gal-9 and TIM-3 in glioblastoma. (A–D) Gal-9 and TIM-3 often co-localized with IBA-1, while the majority of the IBA-1$^+$ cells lacked Gal-9 and TIM-3 expression. (E–F) TIM-3 was frequently co-expressed with Gal-9, while most Gal-9$^+$ cells lacked TIM-3 expression. (G–H) Only a small population of CD3$^+$ T cells expressed TIM-3. (I–L) Most OLIG2$^+$ cells neither expressed Gal-9 nor TIM-3. *Scale bar* 100 μM

3.2 | Association between IDH status and Gal-9 and/or TIM-3 expression in tumor cells

OLIG2$^+$ tumor cells were observed in nearly all specimens and accounted for ~45%–50% of the cells in both IDH-mutant and IDH-wild-type tumors (Figure 3A,B), and no significant IDH-dependent difference was detected (p = 0.58) (Figure 4A and Table 2). Irrespective of IDH status, most OLIG2$^+$ cells did not exhibit membranous TIM-3 or cytoplasmic Gal-9 expression

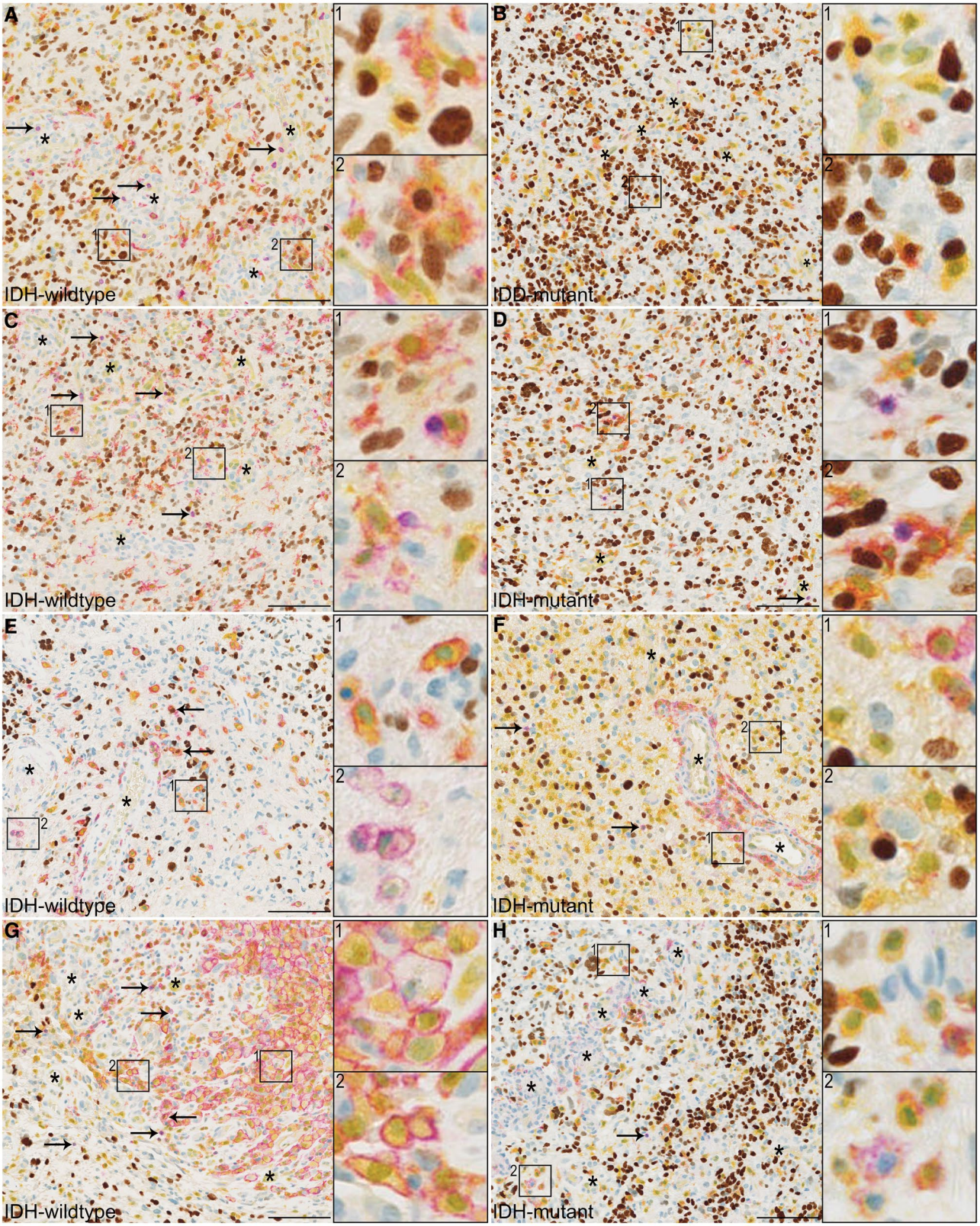

FIGURE 3 Expression patterns of Gal-9, TIM-3, and OLIG2 in IDH-wild-type and IDH-mutant astrocytic gliomas of WHO grades III and IV. (A–B) OLIG2 and Gal-9 were widely expressed in most tumors regardless of IDH mutation status. A weak Gal-9 expression was observed in vascular structures (indicated by *asterisk*). Few TIM-3$^+$ cells were observed, but often resembled either microglia/macrophages or T cells (indicated by *rightward arrows*) with the latter often located in or proximate to vascular structures. Gal-9$^+$ tumor cells (*insert 1*) and Gal-9$^+$ TIM-3$^+$ tumor cells (*insert 2*) were found in both IDH-wild-type and IDH-mutant tumors, although in sparse numbers. (C–D) The percentage of TIM-3$^+$ T cells and the interactions between TIM-3$^+$ T cells and Gal-9$^+$ TAMs (inserts) appeared higher in IDH-wild-type compared to IDH-mutant tumors. (E–H) TIM-3$^+$ cells were more dispersed in IDH-wild-type tumors, while they were more concentrated around blood vessels in IDH-mutant tumors (*asterisks*). Gal-9$^+$ TIM-3$^+$ microglia/macrophages and Gal-9$^-$ TIM-3$^+$ microglia/macrophages appeared to be more prevalent in IDH-wild-type tumors compared to IDH-mutant tumors. *Scale bar* 100 μM. *Asterisk* indicates blood vessels. *Rightward arrows* in (A,C,D,F–H) indicate TIM-3$^+$ T cells. *Leftward arrows* in (E,G) indicate Gal-9$^+$ TIM-3$^+$ tumor cells. *Chromogen colors* brown (OLIG2), purple (TIM-3), yellow (Gal-9), and red (TIM-3 and Gal-9 color mixing)

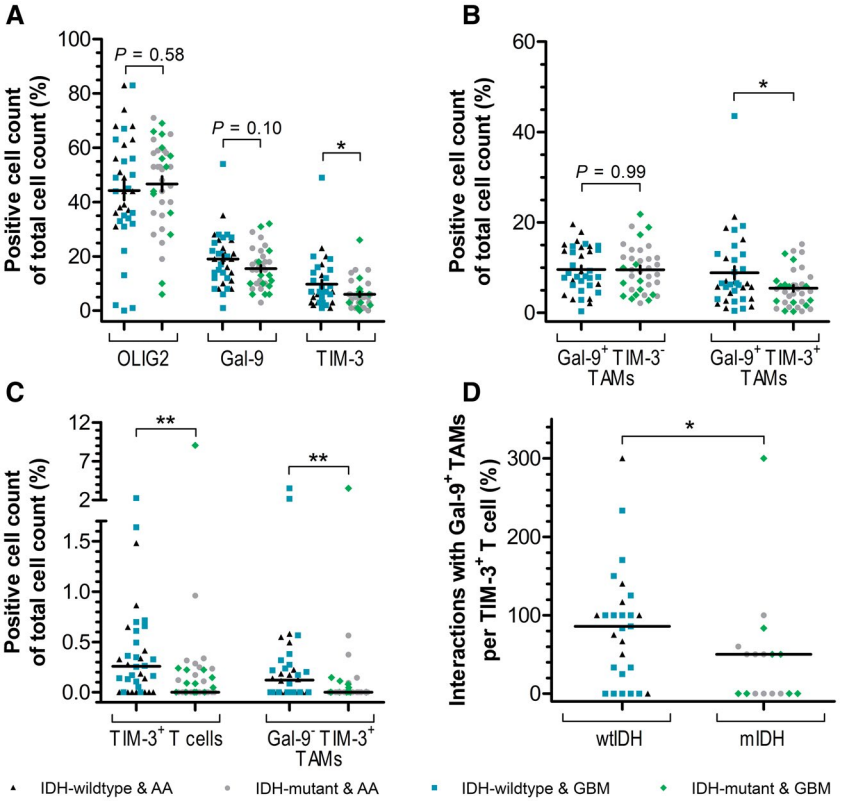

FIGURE 4 Associations between IDH mutation and protein expression of Gal-9, TIM-3, and OLIG2. (A) The percentage of TIM-3$^+$ cells was significantly lower in IDH-mutant tumors compared to IDH-wild-type tumors, while expression levels of OLIG2 and Gal-9 was IDH-independent. (B) The percentage of Gal-9$^+$ TIM-3$^+$ TAMs was lower in IDH-mutant tumors than in IDH-wild-type tumors. (C) The percentages of TIM-3$^+$ T cells and Gal-9$^-$ TIM-3$^+$ TAMs were decreased in IDH-mutant tumors compared to IDH-wild-type tumors. (D) The interaction rate between TIM-3$^+$ T cells and Gal-9$^+$ TAMs was lower in IDH-mutant tumors than in IDH-wild-type tumors. *Horizontal lines* indicate mean (A,B) or median (C,D). *Vertical lines* indicate ± standard error of the mean (SEM) (A, B). *indicates $p < 0.05$; **$p < 0.01$

(mean ± SEM (%): 98.9 ± 0.15 and 98.8 ± 0.20 for IDH-mutant and IDH-wild-type tumors, respectively, $p = 0.73$) (Table 3). About 1% of the OLIG2$^+$ cells expressed Gal-9 in both IDH-mutant and IDH-wild-type tumors (mean ± SEM (%): 0.83 ± 0.14 and 1.04 ± 0.19, respectively, $p = 0.77$) (Figure 3A,B and Table 3), and generally Gal-9$^+$ tumor cells only accounted for ~0.50% of the total cell population (Table 2). TIM-3 was rarely expressed by OLIG2$^+$ cells and only seen when co-expressed with Gal-9 (Figure 3A,B). The presence of TIM-3$^+$ tumor cells was independent of the IDH status (mean ± SEM (%): 0.31 ± 0.08 and 0.19 ± 0.05 for IDH-mutant and IDH-wild-type tumors, respectively, $p = 0.34$) (Table 3). Overall, TIM-3$^+$ tumor cells only comprised ~0.10% of the total cell population (Table 2). Similar results were found when separately analyzing the immunopositivity in the groups of anaplastic astrocytomas and glioblastomas (Table 2 and Table 3). The low expression levels of Gal-9 and TIM-3 in OLIG2$^+$ cells and astrocytic tumor cells in general were confirmed using double immunofluorescence with OLIG2 (Figure 2I–L) or IDH1 R132H (Figure S1). Correlation analyses showed that OLIG2 was negatively correlated with both TIM-3 ($r_s = -0.45$, $p < 0.05$) and Gal-9 ($r_s = -0.54$, $p < 0.01$) (Figure S2A)

TABLE 2 Summary of the immunostaining results for all cell populations

	Anaplastic astrocytoma		Glioblastoma		All astrocytic gliomas	
	WHO grade III		WHO grade IV		WHO grade III-IV	
	wtIDH	mIDH	wtIDH	mIDH	wtIDH	mIDH
	n = 16	*n* = 23	*n* = 19	*n* = 14	*n* = 35	*n* = 37
Total OLIG2$^+$ cells						
Mean ± SEM (%)	52.6 ± 3.87	47.3 ± 2.86	37.6 ± 5.02	45.6 ± 5.71	44.3 ± 3.47	46.7 ± 2.71
Median (%)	50.0	52.0	35.5	53.0	44.0	52.5
p-value		0.27[a]		0.31[a]		0.58[a]
Total Gal-9$^+$ cells						
Mean ± SEM (%)	19.0 ± 1.92	16.1 ± 1.34	19.0 ± 2.55	14.4 ± 2.47	19.0 ± 1.63	15.5 ± 1.22
Median (%)	19.0	16.0	18.5	11.0	19.0	15.0
p-value		0.21[a]		0.19[b]		0.10[b]
Total TIM-3$^+$ cells						
Mean ± SEM	8.13 ± 1.65	5.83 ± 0.93	11.0 ± 2.36	6.31 ± 1.86	9.69 ± 1.50	6.00 ± 0.88
Median	6.50	5.00	8.00	6.00	7.00	5.00
p-value		0.20[a]		0.061[b]		**0.024**[b]
Gal-9$^-$ TIM-3$^-$ tumor cells						
Mean ± SEM (%)	51.8 ± 3.74	46.8 ± 2.82	37.0 ± 4.95	45.1 ± 5.65	43.6 ± 3.40	46.2 ± 2.67
Median (%)	49.5	51.0	35.1	52.4	43.2	51.6
p-value		0.43[a]		0.30[a]		0.55[a]
Gal-9$^+$ TIM-3$^-$ tumor cells						
Mean ± SEM (%)	0.64 ± 0.16	0.41 ± 0.09	0.44 ± 0.13	0.35 ± 0.11	0.53 ± 0.10	0.39 ± 0.07
Median	0.46	0.30	0.17	0.24	0.24	0.29
p-value		0.50[b]		0.97[b]		0.73[b]
Gal-9$^+$ TIM-3$^+$ tumor cells						
Mean ± SEM (%)	0.10 ± 0.05	0.11 ± 0.04	0.09 ± 0.03	0.15 ± 0.04	0.09 ± 0.03	0.13 ± 0.03
Median (%)	0.00	0.00	0.00	0.15	0.00	0.04
p-value		0.73[b]		0.16[b]		0.33[b]
Gal-9$^+$ TIM-3$^-$ TAMs						
Mean ± SEM (%)	10.7 ± 1.45	9.91 ± 0.87	8.57 ± 0.93	8.81 ± 1.81	9.54 ± 0.83	9.51 ± 0.84
Median (%)	13.08	9.85	7.92	6.55	8.40	9.36
p-value		0.60[a]		0.90[a]		0.99[a]
Gal-9$^+$ TIM-3$^+$ TAMs						
Mean ± SEM (%)	7.48 ± 1.57	5.61 ± 0.89	9.89 ± 2.15	5.02 ± 1.11	8.82 ± 1.38	5.40 ± 0.69
Median (%)	5.71	4.75	6.82	5.79	6.35	5.00
p-value		0.32[b]		0.068[b]		**0.044**[b]
Gal-9$^-$ TIM-3$^+$ TAMs						
Mean ± SEM	0.16 ± 0.05	0.05 ± 0.03	0.41 ± 0.20	0.30 ± 0.27	0.30 ± 0.11	0.14 ± 0.10
Median	0.12	0.00	0.13	0.00	0.12	0.00
p-value		**0.014**[b]		0.16[b]		**0.004**[b]
TIM-3$^+$ T cells						
Mean ± SEM (%)	0.29 ± 0.10	0.12 ± 0.05	0.47 ± 0.13	0.77 ± 0.69	0.39 ± 0.28	0.36 ± 0.25
Median (%)	0.16	0.00	0.29	0.10	0.26	0.00
p-value		0.13[b]		**0.014**[b]		**0.002**[b]
Interactions with Gal-9$^+$ tumor cell per TIM-3$^+$ T cell						
Mean ± SEM	2.22 ± 2.22	11.1 ± 11.1	6.48 ± 5.58	0.00 ± 0.00	5.06 ± 3.77	5.88 ± 5.88

(Continues)

TABLE 2 (Continued)

	Anaplastic astrocytoma		Glioblastoma		All astrocytic gliomas	
	WHO grade III		WHO grade IV		WHO grade III-IV	
	wtIDH	mIDH	wtIDH	mIDH	wtIDH	mIDH
	n = 16	*n* = 23	*n* = 19	*n* = 14	*n* = 35	*n* = 37
Median	0.00	0.00	0.00	0.00	0.00	0.00
p-value		1.00[b]		–		0.61[b]
Interactions with Gal-9$^+$ TAMs per TIM-3$^+$ T cell						
Mean ± SEM	105 ± 27.8	34.4 ± 12.0	74.4 ± 16.1	60.4 ± 36.0	84.7 ± 14.2	46.7 ± 17.8
Median	100	50.0	84.5	25.0	85.7	50.0
p-value		**0.017**[b]		0.28[b]		**0.025**[b]

Bold values indicate that the difference is significant ($p < 0.05$),

Abbreviations: mIDH, IDH-mutant; TAMs, tumor-associated microglia/macrophages; wtIDH, IDH-wild-type.

[a]Student's *t*-test.

[b]Mann–Whitney *U*-test.

suggesting that the tumor cell density was lower in tumors and/or tumor areas with high levels of TIM-3 and Gal-9 expression.

3.3 | Association between IDH status and expression of Gal-9 and/or TIM-3

Gal-9 was widely distributed in all tumors and also weakly expressed by most blood vessels (Figure 3A–D). The overall percentage of Gal-9$^+$ cells tended to be lower in IDH-mutant than in IDH-wild-type tumors ($p = 0.10$) accounting for ~15% and ~20% of all cells, respectively (Figure 4A and Table 2). TIM-3$^+$ cells were often found around vascular structures in IDH-mutant tumors (Figure 3F,H), while they were detected both perivascularly as well as in a more dispersed manner in IDH-wild-type tumors (Figure 3E,G). The TIM-3$^+$ cell population was significantly lower in IDH-mutant than in IDH-wild-type tumors ($p = 0.024$) contributing with ~6% and ~10% of the total cell count, respectively. Spearman's correlation analysis showed a strong positive correlation between the percentages of Gal-9$^+$ and TIM-3$^+$ cells ($r_s = 0.73$, $p < 0.0001$) (Figure S2A,B).

3.4 | Association between IDH status and expression of Gal-9 and/or TIM-3 in tumor-associated immune cells

Gal-9$^+$ TIM-3$^-$ TAMs comprised ~10% of the cells in both IDH-mutant and IDH-wild-type tumors ($p = 0.99$), whereas the percentage of Gal-9$^+$ TIM-3$^+$ TAMs was lower in IDH-mutant tumors compared to IDH-wild-type tumors (~5% vs. 9%, respectively, $p = 0.044$) (Figure 4B and Table 2). The presence of Gal-9$^-$ TIM-3$^+$ TAMs were generally low irrespective of the IDH status, however, the percentage was significantly lower in IDH-mutant tumors (~0.15% vs. 0.30%, $p = 0.004$) (Figure 4C and Table 2). Similarly, TIM-3$^+$ T cells were rarely found, but the median percentage was significantly lower in IDH-mutant tumors (0.00% vs. 0.26%, $p = 0.002$) (Figure 4C and Table 2). Almost none of the TIM-3$^+$ T cells interacted with Gal-9$^+$ tumors cells. In contrast, ~85%–100% of TIM-3$^+$ T cells interacted with Gal-9$^+$ TAMs in IDH-wild-type tumors, whereas a 50% interaction rate was found in IDH-mutant tumors ($p = 0.025$) (Figures 3C,D, 4D and Table 2). Similar outcomes/tendencies were obtained when stratifying according to WHO grade and IDH status.

Looking only at the population of TAMs, the percentage of Gal-9$^+$ TIM-3$^+$ TAMs was significantly lower in IDH-mutant compared to IDH-wild-type tumors (mean ± SEM (%): 34.7 ± 3.12 and 44.1 ± 3.49, $p = 0.048$) (Table 3). TIM-3$^+$ TAMs often appeared ameboid and had a large cytoplasm that expressed Gal-9 to varying extents (Figure 3E–H). Inversely, the percentage of Gal-9$^+$ TIM-3$^-$ TAMs was significantly higher in IDH-mutant compared to IDH-wild-type tumors (mean ± SEM (%): 64.6 ± 3.14 and 54.4 ± 3.49, respectively, $p = 0.033$). Few Gal-9$^-$ and TIM-3$^+$ TAMs were seen, accounting for <1% of the TAM population, but the actual percentage was significantly lower in IDH-mutant tumors ($p = 0.012$) (Table 3). Similar results/tendencies were found stratifying based on WHO grade and IDH status (Table 3).

Next, we investigated the association between Gal-9/TIM-3 expression and the different T cell populations by performing correlation analyses using the CD4, CD8, and FOXP3 immunostaining results from our previous study (37). Both Gal-9 and TIM-3 positively correlated with all three T cell markers (CD4: $r_s = 0.51$ and $r_s = 0.53$, $p < 0.001$; CD8: $r_s = 0.58$ and $r_s = 0.52$, $p < 0.001$; and FOXP3: $r_s = 0.42$ and $r_s = 0.49$, $p < 0.001$) (Figure S2A).

3.5 | *In silico* analyses of TCGA data sets

To explore the impact of IDH status on the expression levels of *Gal-9* and *TIM-3* at the transcriptional level, we

TABLE 3 Summary of the immunostaining results for tumor cells and TAMs

	Anaplastic astrocytoma		Glioblastoma		All astrocytic gliomas	
	WHO grade III		WHO grade IV		WHO grade III-IV	
	wtIDH	mIDH	wtIDH	mIDH	wtIDH	mIDH
	n = 16	*n* = 23	*n* = 19	*n* = 14	*n* = 35	*n* = 37
Tumor cells[a]						
Gal-9$^-$ and TIM-3$^-$						
Mean ± SEM	98.8 ± 0.28	98.9 ± 0.17	98.8 ± 0.29	98.9 ± 0.29	98.8 ± 0.20	98.9 ± 0.15
Median	98.7	99.0	99.3	99.1	99.1	99.1
p-value		0.97[b]		0.89[a]		0.73[a]
Gal-9$^+$ and TIM-3$^-$						
Mean ± SEM	1.09 ± 0.25	0.88 ± 0.18	0.99 ± 0.28	0.75 ± 0.20	1.04 ± 0.19	0.83 ± 0.14
Median	1.09	0.74	0.48	0.50	0.60	0.64
p-value		0.63[b]		0.99[b]		0.77[b]
Gal-9$^+$ and TIM-3$^+$						
Mean ± SEM	0.16 ± 0.07	0.26 ± 0.10	0.21 ± 0.07	0.39 ± 0.14	0.19 ± 0.05	0.31 ± 0.08
Median	0.00	0.00	0.00	0.28	0.00	0.07
p-value		0.65[b]		0.21[b]		0.34[b]
TAMs[d]						
Gal-9$^+$ and TIM-3$^-$						
Mean ± SEM	59.2 ± 6.16	66.5 ± 3.88	50.6 ± 3.83	61.3 ± 5.40	54.4 ± 3.49	64.6 ± 3.14
Median	65.7	68.2	52.9	57.9	54.6	64.0
p-value		0.30[a]		0.11[a]		**0.033**[a]
Gal-9$^+$ and TIM-3$^+$						
Mean ± SEM	39.9 ± 6.11	33.1 ± 3.92	47.5 ± 3.93	37.5 ± 5.28	44.1 ± 3.49	34.7 ± 3.12
Median	34.3	31.8	44.9	39.7	43.0	36.0
p-value		0.33[a]		0.13[a]		**0.048**[a]
Gal-9$^-$ and TIM-3$^+$						
Mean ± SEM	0.92 ± 0.26	0.44 ± 0.28	1.94 ± 0.79	1.17 ± 0.78	1.49 ± 0.46	0.70 ± 0.34
Median	0.68	0.00	0.57	0.00	0.67	0.00
p-value		**0.021**[b]		0.39[b]		**0.012**[b]

Bold values indicate that the difference is significant ($p < 0.05$),

Abbreviations: mIDH, IDH-mutant; TAMs, tumor-associated microglia/macrophages; wtIDH, IDH-wild-type.

[a]Student's *t*-test.

[b]Mann–Whitney *U*-test.

[c]Tumor cells were defined as OLIG2$^+$ cells.

[d]TAMs were defined as OLIG2$^-$, Gal-9$^{+/-}$ and TIM-3$^{-/+}$ cells with microglial/macrophage-like morphology.

performed *in silico* analyses based on data provided in the TCGA database (http://gliovis.bioinfo.cnio.es/). In line with our immunohistochemical findings, IDH-mutant astrocytic gliomas of WHO grade III and IV showed a lower *TIM-3* mRNA expression compared to corresponding IDH-wild-type astrocytic gliomas ($p = 0.013$). A similar tendency was seen for *Gal-9* expression levels ($p = 0.074$). Similar to the protein data, a strong positive correlation was found between *Gal-9* and *TIM-3* mRNA expression levels (r_s =0.88, $p < 0.0001$). Furthermore, *Gal-9* and *TIM-3* mRNA levels were positively correlated to mRNA expression levels of *CD4* ($r_s = 0.85$ and $r_s = 0.87$, respectively, $p < 0.001$), *CD8A* ($r_s = 0.36$ and $r_s = 0.40$, respectively, $p < 0.001$), *CD8B* ($r_s = 0.43$ and $r_s = 0.44$, respectively, $p < 0.001$), and *FOXP3* ($r_s = 0.32$ and $r_s = 0.23$, respectively, $p < 0.001$). (Figure S2C,D). In contrast to the protein data, *OLIG2* mRNA expression was significantly higher in IDH-mutant than in IDH-wild-type tumors (Figure 5A), and like the protein data, *OLIG2* mRNA levels showed a weak to moderate negative correlation with mRNA expression levels of *Gal-9*, *TIM-3* and the T cell markers (Figure S2C).

To further investigate the influence of IDH mutation on the immune landscape in glioma, we included IDH-mutant and IDH-wild-type diffuse astrocytomas, WHO grade II, as well as IDH-mutant and 1p/19q-codeleted

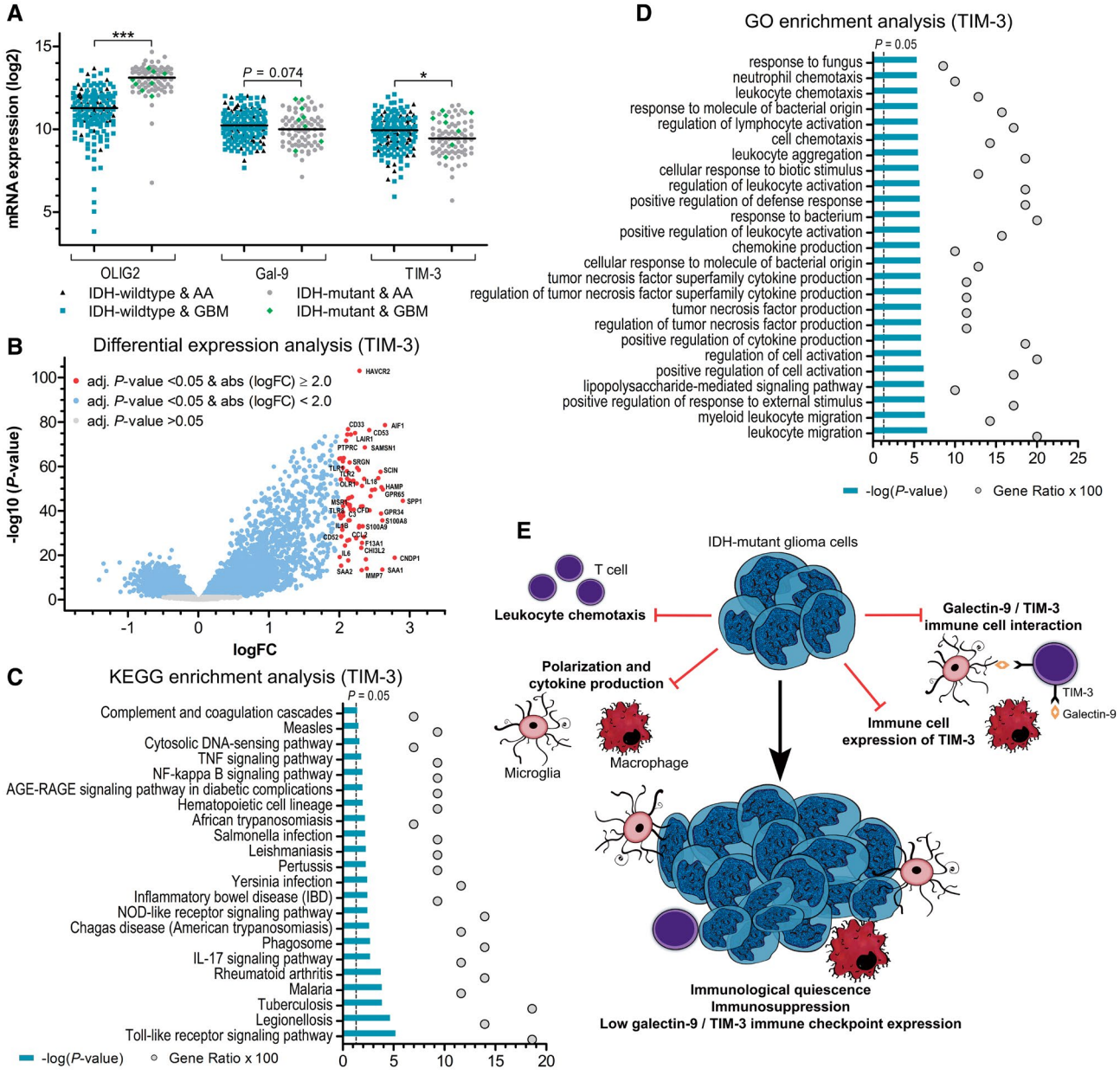

FIGURE 5 TCGA, differential expression analyses, and pathway enrichment analyses. (A) Association between IDH mutation status and *OLIG2*, *Gal-9*, and *TIM-3* expression levels in the TCGA data set. (B) Volcano plot illustrating the 75 genes (red dots) that were significantly upregulated ≥2.00-fold threshold in *TIM-3*^{HIGH} versus *TIM-3*^{LOW} glioblastoma samples. (C,D) The upregulated genes were hierarchically classified according to biological processes and pathways using the Kyoto Encyclopedia of Genes and Genomes (KEGG) (C) and Gene Ontology (GO) term (D) enrichment analyses. (E) Schematic illustration of the possible immunomodulatory of IDH mutation in glioma. IDH mutation and its oncometabolite D-2-hydroxyglutarate may cause suppression of leukocyte chemotaxis and microglia/macrophage polarization as well as cytokine production thereby reducing the expression and activity of the galectin-9/TIM-3 immune checkpoint pathway. *Horizontal lines* indicate median (A). *indicates $p < 0.05$; ***$p < 0.001$

oligodendrogliomas, WHO grade II and III, in our *in silico* analyses. Oligodendrogliomas, WHO grade II, overall exhibited the lowest mRNA expression level of both *Gal-9* and *TIM-3* ($p < 0.001$) among the glioma subtypes. Interestingly, no significant difference was observed between IDH-wild-type WHO grade II or III astrocytomas and WHO grade IV glioblastoma for either *Gal-9* or *TIM-3*, while IDH-mutant WHO grade II and III astrocytomas had significantly lower mRNA expression levels of *Gal-9* ($p < 0.05$) and *TIM-3* ($p < 0.001$) compared to IDH-wild-type glioblastoma of WHO grade IV (Figure S3A,B). We also examined the mRNA expression levels of the T cell markers *CD4*, *CD8A*/*B*, and *FOXP3* among the different glioma subtypes. WHO grade II–III oligodendroglial tumors had significantly lower *CD4* levels compared to the astrocytic tumors ($p < 0.001$) independent of IDH status. Among the astrocytic gliomas, IDH-mutant WHO grade II and III tumors had lower *CD4* levels compared to IDH-wild-type glioblastomas ($p < 0.05$) (Figure S3C). Oligodendroglial tumors as well

as IDH-mutant astrocytic gliomas including glioblastomas had significantly lower *CD8A*/*B* expression levels compared to IDH-wild-type astrocytic tumors (Figure S3D,E). In contrast, *FOXP3* expression levels were highest in oligodendroglial tumors, followed by IDH-wild-type astrocytomas/glioblastomas (Figure S3F). As our double immunofluorescence stainings showed that most Gal-9$^+$ and TIM-3$^+$ co-expressed IBA-1, we explored the association between glioma subtype including IDH status and *IBA-1* mRNA expression. We found that oligodendroglial tumors had significantly lower *IBA-1* levels than astrocytic tumors, irrespective of IDH status and WHO grade ($p < 0.001$), while no significant differences were observed among the astrocytic subgroups (Figure S4A) despite the fact that *IBA-1* was positively correlated to both mRNA *Gal-9* ($r_s = 0.88$, $p < 0.001$) and mRNA *TIM-3* ($r_s = 0.92$, $p < 0.001$) in glioma (Figure S4B,C).

As *TIM-3* mRNA expression was consistently lower in IDH-mutant gliomas, we employed the TCGA data set to screen for changes in mRNA levels of 17,811 genes between the glioblastomas with the highest and lowest *TIM-3* mRNA levels. A total of 75 genes were found to be differentially upregulated (FC ≥ 2.00) in glioblastomas with the highest *TIM-3* mRNA level (Figure 5B and Table S2), while no genes were differentially downregulated with a twofold change threshold. Several of the upregulated genes were related to microglia/macrophage migration, chemotaxis, and/or polarization (69–73), including *SPP1*, *IBA-1*, *CD204*, *IL1B*, *IL6*, *IL18*, and *CCL2* as well as *TLR1*, *TLR2*, and *TLR8*. Exploratory analyses showed that the mRNA expression of these microglial/macrophage genes, except *IBA-1*, was significantly lower in WHO grade III and IV IDH-mutant astrocytic gliomas compared to their IDH-wild-type counterparts (Figure S5), and the mRNA results were validated for IBA-1 and CD204 at a protein level using immunohistochemistry (Figure S5). KEGG and GO enrichment analyses were used to generate a biological and functional profile of the differentially regulated genes. The differentially upregulated genes were significantly enriched in the signaling pathways of TLR, IL17, nucleotide-binding oligomerization domain-like (NOD-like) receptor, nuclear factor-kappa B (NFκB), and TNF as well as in the phagosome pathway and various inflammatory/infectious diseases (Figure 5C and Table S3). Further, the upregulated genes were involved in biological processes such as leukocyte migration, regulation and aggregation as well as regulation of cell activation and production of cytokines including the tumor necrosis factor (TNF) superfamily (Figure 5D and Table S4).

4 | DISCUSSION

This study reports that IDH mutation is related to overall decreased expression levels of TIM-3 and fewer TIM-3$^+$ immune cells in human astrocytoma tissues. Furthermore, a significantly lower interaction rate between TIM-3$^+$ T cells and Gal-9$^+$ TAMs was detected in IDH-mutant anaplastic astrocytomas and glioblastomas, suggesting that the Gal-9/TIM-3 checkpoint pathway could be suppressed to a higher degree compared to IDH-wildtype tumors.

TIM-3 is a type I transmembrane glycoprotein that contains a variable immunoglobulin domain and a mucin-like domain. It was initially identified on differentiated CD4$^+$ T helper type 1 cells (74), and is also expressed by other subtypes of lymphoid cells, monocytes/macrophages, dendritic cells, and distinct types of cancer cells. TIM-3 expression is upregulated when stimulated by antigens and in response to pro-inflammatory cytokines. TIM-3 negatively regulates T cell activation, is involved in T cell exhaustion along with PD-1, and contributes to tumor-induced immune suppression by binding to its ligand Gal-9 (45, 48). Combined targeting of TIM-3 and PD-1 was able to restore tumor-infiltrating lymphocyte (TIL) function (51). In myeloid cells, TIM-3 has been shown to regulate cytokine production, cell activation, and capture of apoptotic bodies (52).

We found that IDH mutation was associated with fewer TIM-3$^+$ cells in astrocytic gliomas and lower *TIM-3* mRNA levels in gliomas. Using the TCGA data set, glioblastomas with high *TIM-3* mRNA levels showed upregulation of a distinct gene set including genes encoding macrophage/immune-related markers, such as *IBA-1*, *CD204*, *SPP1*, *CCL2*, *IL6*, *IL18*, and *IL1B* as well as *TLR1*, *TLR2*, and *TLR8*. The upregulated genes were involved in regulation of biological processes of the immunocyte including migration, activation, chemotaxis, and cytokine/chemokine production. KEGG enrichment analyses of upregulated genes showed categories such as the TNF and NFκB signaling pathways which have been associated with shaping of the extracellular matrix and tumor invasiveness in glioblastoma (73, 75). Additionally, the TLR and IL17 signaling pathways were enriched in glioblastomas with high *TIM-3* expression. Dependent on the stimulated receptor, the cell type, and the microenvironment, these pathways can exhibit both pro- and antitumor properties either by facilitating antigen presentation and stimulating innate and adaptive immunity or by promoting an immunosuppressive tumor microenvironment, respectively (76–79). These findings are in agreement with analyses performed on RNA-seq data from patients with glioma where *TIM-3* was associated with IDH-wild-type tumors, mesenchymal glioblastoma, poorer performance status, and shorter survival (56, 58, 59). Investigating the TIM-3 expression on peripheral innate immune cells, Li et al. found that monocytes and natural killer (NK) cells had higher TIM-3 expression in glioma patients compared to healthy controls, despite the fact that the overall level of circulating NK cells was reduced in patients. In glioma patients, the TIM-3$^+$ NK cells showed a diminished ability to secrete their antitumor effector molecule interferon-γ (IFNG),

while the TIM-3$^+$ monocytes exhibited a pro-tumorigenic M2-like phenotype compared to healthy controls (59). In a recent meta-analysis that included seven studies on carcinomas, high TIM-3 expression was found to be significantly associated with shorter overall survival and more advanced tumor stage (80). Overall, these results indicate that TIM-3 could facilitate tumor progression and aggressiveness.

We observed that the frequency of Gal-9$^+$ cells was not significantly affected by IDH status in WHO grade III and IV astrocytic gliomas. However, we observed a trend toward a lower percentage of Gal-9$^+$ cells in IDH-mutant tumors. Using data from three RNA-seq cohorts, Liang et al. reported that *Gal-9* expression was downregulated in high-grade gliomas with mutant IDH, while no significant IDH-dependent difference was seen in low-grade gliomas (55). This inconsistency in results could be explained by the inclusion of IDH-mutant and 1p/19q-codeleted oligodendroglial tumors in the study by Liang et al. as these tumors are more immunologically quiet than IDH-mutant noncodeleted astrocytic tumors (28, 65, 81), and in our *in silico* TCGA analyses we found that oligodendroglial tumors had the lower expression levels of *Gal-9* compared to astrocytic gliomas. Consistent with studies by Liang et al. (55) and Liu et al (56), we observed a strong positive correlation between Gal-9 and TIM-3 immunoreactivity. Like TIM-3, Gal-9 has been linked to poorer prognosis and the aggressive mesenchymal subtype of glioblastoma (55, 57). In contrast, OLIG2 has been associated with the proneural subtype of high-grade gliomas (61, 82, 83), and thus, IDH mutations (83, 84). Surprisingly, no association between OLIG2 and IDH mutation was found at the protein level, while IDH-mutant anaplastic astrocytomas and glioblastomas expressed higher *OLIG2* mRNA levels compared to the respective IDH-wildtype tumors in the TCGA data set. The observed discrepancy between protein and mRNA results could be explained by translational regulation (85, 86), and can also be attributed to the sensitivity of OLIG2 antibody used in our study. Further, only the number of OLIG2$^+$ cells was evaluated, but not the staining intensity which could also contribute to the overall OLIG2 expression level in the tissue.

We analyzed an immune checkpoint pathway using a new emerging method for detection of multiple biomarkers within a single tissue section (87–90). Using this brightfield multiplex chromogenic immunohistochemistry methodology; we were able to decipher three dyes while preserving tissue morphology and architecture without any loss of antigenicity and only limited steric interference and cross-reactivity. We validated the reliability of the chromogenic color mixing using double immunofluorescence. The present study, however, had some limitations. The quantification was done using a stereological approach as digital automated quantification was not feasible because of the overlap of the chromogenic spectra and the detail level that would be acquired by our image analysis. Also, stereology is often a very time-consuming process limiting the usability of chromogenic multiplexing in clinical pathology. Moreover, our choice for selected markers was limited when developing the multiplex panel because of both technical and antigen-specific aspects. Thus, while chromogenic multiplexing can be a valuable tool, the ability to multiplex beyond three targets/antigens is limited in practice (90). Most studies performing multiplexed imaging to examine the tumor immune microenvironment use multiplex immunofluorescence (91, 92) which allows for combining up to 12 fluorophores (90). However, cellular morphology and tissue context are often more difficult to evaluate in fluorescent stains compared to chromogenic stains, presenting a disadvantage in using fluorescent multiplexing.

In our study, most Gal-9$^+$ and TIM-3$^+$ cells morphologically resembled microglia/macrophages, while a weak expression also was observed in vascular structures. Reportedly, Gal-9 expression can be induced by IFNG or IL1B in various cells such as endothelial cells, T cells, astrocytes, and neurons (93–97), while ischemia was found to induce TIM-3 expression by astrocytes (98). In our study, cells were denoted as microglia/macrophages based on morphological features. This presents a possible drawback as microglia and reactive astrocytes as well as ameboid macrophages and gemistocytic tumor cells, respectively, can be difficult to discriminate morphologically. To address this aspect, we performed double immunofluorescence and confirmed that on average 80% of Gal-9$^+$ and TIM-3$^+$ area co-expressed the microglial/macrophage marker IBA-1. Gal-9 expression in glioma cells was reported by Liu et al. (56), however, we observed very few Gal-9 expressing tumor cells, and even fewer tumor cells that expressed TIM-3. Our findings were validated by double immunofluorescence as only ~1% and ~0.1% of the OLIG2$^+$ tumor cells co-expressed Gal-9 and TIM-3, respectively. We used OLIG2 to denote tumor cells instead of, for example, glial fibrillary acidic protein (GFAP) because of its nuclear localization and distinct expression making it feasible to perform chromogenic multiplexing with the cytoplasmic Gal-9 and membranous TIM-3. OLIG2 is expressed in most gliomas and glioblastomas, but only in a subset of tumor cells thus introducing a caveat in our study, as the level of Gal-9 and/or TIM-3 expressing tumor cells may be underestimated. To address this limitation, we performed double immunofluorescence with an antibody against the tumor cell-specific IDH1 R132H mutant protein. These stainings supported our finding, demonstrating that Gal-9 and TIM-3 expression is rare in glioma cells.

Similarly to Gal-9$^+$ cells, most TIM-3$^+$ cells had microglial/macrophage-like morphology, and TIM-3 was almost consistently co-expressed with Gal-9. A few cells expressed TIM-3 only, and these cells resembled either lymphocytes or microglia/macrophages. Less than 0.5% of cells were TIM-3$^+$ T cells, and only ~ 10% of the CD3$^+$

T cell population in glioblastoma expressed TIM-3. This is in agreement with work performed by others (49, 56, 99–101). Using flow cytometry, Han et al reported that $CD3^+$ T cells were a rare population in glioblastomas accounting for less than 0.25% of the cells (100). Among the T cell populations ~ 6%–12% and ~ 4%–6% of the $CD8^+$ and $CD4^+$ TILs were found to express TIM-3, respectively (56, 99, 101). Despite their rarity in glioma, TIM-3^+ TILs could play an important part in the immunosuppressive microenvironment in glioma. Reportedly, TIM-3 expression has been shown to contribute to an immune signature of exhaustion in TILs (51), also in glioblastoma patients (49, 101), and together with PD-1 expression was found to increase over time in murine gliomas (102) suggesting that TIM-3 may be upregulated during gliomagenesis representing an immunosuppressive adaptation. Additionally, TIM-3^+ T cells correlated with increased tumor grade and poorer performance status (49, 99), overall suggesting an association with tumor aggressiveness. Further, TIM-3 blockade combined with PD-1 blockade and radiation was demonstrated to improve survival in murine glioma compared with dual or monotherapy, and combination therapy was able to restore the anti-tumorigenic functions of T cells (102). In the clinical setting, a phase 1 trial (NCT03961971) has been scheduled in recurrent glioblastoma, combining the anti-TIM-3 inhibitor MBG453 with the PD-1 inhibitor spartalizumab and stereotactic radiosurgery (47).

We observed significantly lower percentages of Gal-$9^{+/-}$ TIM-3^+ TAMs and TIM-3^+ T cells in WHO grade III anaplastic astrocytomas and WHO grade IV glioblastomas with IDH mutation compared to their IDH-wild-type counterparts. Interestingly, we found that most TIM-3^+ cells resembled TAMs. Almost half of the Gal-9^+ TAMs co-expressed TIM-3 in WHO grade III–IV IDH-wild-type astrocytic gliomas, while only a third of the Gal-9^+ TAMs co-expressed TIM-3 in WHO grade III–IV IDH-mutant astrocytic gliomas. Co-expression of Gal-9 and TIM-3 has also been observed in human acute myeloid leukemia cells (103, 104) and human breast cancer cells (105), possibly forming an autocrine loop that promotes self-renewal and immune evasion. In monocytes and macrophages, the specific association of Gal-9 with TIM-3 was reported to differentially regulate TLR activation, IL12/IL23 production, and Gal-9/TIM-3 surface expression depending on whether TIM-3 was expressed by other cells (*trans*) or on the monocyte/macrophage itself (*cis*) (106). This suggests that our observed Gal-9 and TIM-3 expression pattern by microglia/macrophages could constitute an intricate autocrine and paracrine signaling loop which may ultimately impact the general activity level of the immune checkpoint pathway. Also, we found a reduced interaction rate between TIM-3^+ T cells and Gal-9^+ TAMs in IDH-mutant compared to IDH-wild-type astrocytic gliomas. Overall, our findings suggest that the expression and possibly activation of the Gal-9/TIM-3 immune checkpoint pathway may be compromised in astrocytic gliomas that carry an IDH mutation. It is unknown whether this is specifically because of the fewer number of TIM-3^+ T cells and/or microglia/macrophages or is a result of an overall reduced level of these immune cells in IDH-mutant tumors. We attempted to address this aspect by correlating protein and/or mRNA expression levels of TIM-3 and Gal-9 to the T cell markers, CD4 (T helper cells), CD8 (cytotoxic T cells), and FOXP3 (regulatory T cells) as well as the microglial/macrophage marker IBA-1. Gal-9 and TIM-3 expression were only weakly to moderately correlated with T cell levels, but showed strong positive correlation with microglia/macrophage levels. This suggests that the decrease in TIM-3^+ cells in IDH-mutant tumors could be because of a lower level of especially microglia/macrophages as the majority of TIM-3^+ cells co-expressed IBA-1. However, as opposed to T cell levels, mRNA and protein IBA-1 expression did not depend on IDH mutation status in astrocytic gliomas, overall indicating that the regulation of the Gal-9/TIM-3 checkpoint pathway is complex and multifactorial. In contrast to IBA-1, genes related to both M1- and M2 polarization, for example, CD204 were significantly lower in IDH-mutant astrocytic gliomas (69–73), suggesting innate immune activation is suppressed in tumors carrying an IDH mutation.

Several studies have reported on the immunomodulating effects of IDH mutation and its oncometabolite D-2-hydroxyglutarate functioning as an intercellular inhibitor of both the innate and adaptive immune systems. Recently, D-2-hydroxyglutarate was found to inhibit the activation of complement in both the classical and the alternative pathways and also shown to compromise the activity of T cells. Furthermore, IDH-mutant WHO grade III–IV astrocytic gliomas generally contained fewer $CD4^+$ TILs, $CD8^+$ TILs, and regulatory TILs compared to their IDH-wild-type counterparts (37). Similar results on TILs have been reported by others (20, 28, 31–33, 35). Studies have also shown that the expression of the immunosuppressive molecule and immune checkpoint marker programed death protein ligand 1 (PD-L1) is diminished in IDH-mutant gliomas relative to IDH-wild-type gliomas, possibly because of epigenetic regulation and suppression mediated by D-2-hydroxyglutarate (32, 42). Further, in a study by Gao et al. immunophenotyping showed that WHO grade II gliomas, which predominantly harbored an IDH mutation, had an immunophenogram that was different from glioblastomas and correlated with poorer response to checkpoint inhibition (34, 107). Bunse et al. demonstrated that oral administration of an IDH inhibitor in combination with R132H peptide vaccination, adoptive T lymphocyte immunotherapy, or PD-1 blockade had synergistic effects and resulted in increased overall survival in a syngeneic orthotopic IDH-mutant mouse model (33), suggesting that combining immunotherapy with IDH inhibition could have clinical relevance. IDH-mutant glioma cells were also reported to resist NK cell-mediated lysis by silencing expression of

NK group 2D ligands through D-2-hydroxyglutarate-induced hypermethylation (41). IDH mutation status may also affect the presence and function of microglia/macrophages in gliomas as lower quantities were found in IDH-mutant gliomas, especially oligodendrogliomas (20, 31, 81). Interestingly, α-ketoglutarate, the normal product from the IDH-catalyzed reaction, was found to prevent M1 activation and enhance M2 polarization in macrophages thereby facilitating tumor progression and development (38). A decline in α-ketoglutarate and indirectly an increase in D2-hydroxyglutarate levels in IDH-mutant gliomas may thus favor anti-tumorigenic M1 activation in microglia/macrophages. Overall, these data indicate that the tumor microenvironment is more immunosuppressive in gliomas harboring an IDH mutation compared to their wildtype counterparts. This seems somewhat counterintuitive as IDH mutation has been associated with a survival benefit in patients with glioma. In a recent study by Unruh et al. (22), the patterns of DNA methylation and transcriptome profiles were investigated in IDH-mutant cancers including glioma. The IDH mutation-induced hypermethylation was found to be more pronounced in gliomas compared to other cancers, and gene set enrichment analyses of IDH-mutant versus IDH-wildtype gliomas revealed downregulation of multiple biological processes in IDH-mutant gliomas; the most notable processes were tissue development, immune response, angiogenesis, and cell proliferation which are all considered to contribute to tumor aggressiveness (40, 67, 82, 83). Taken together, research indicates that IDH mutation promotes an immunoquiescent tumor microenvironment.

5 | CONCLUSION

The success of immunotherapy in glioma faces several obstacles including a lymphocyte-depleted and immunosuppressive tumor microenvironment as well as the limitations of effectively generating an immune response in the central nervous system. Increasing evidence suggests that mutations in IDH play an essential role in glioma-associated immune suppression. The neomorphic activity of mutant IDH results in accumulation of D-2-hydroxyglutarate which has been implicated in DNA hypermethylation, ultimately promoting global repression of several genes including those involved in stimulating antitumor immune responses. Reportedly, the activity of the innate and adaptive immune system including the checkpoint systems is reduced in gliomas harboring an IDH mutation. Our results demonstrate that the Gal-9/TIM-3 checkpoint pathway is affected by IDH mutation as the overall level of TIM-3 expression was diminished in IDH-mutant astrocytic gliomas. Additionally, fewer receptor-ligand interactions was observed as the interaction rate between TIM-3^+ T cells and Gal-9^+ microglia/macrophages were less frequent in IDH-mutant tumors (Figure 5E). Collectively, these results indicate that IDH mutation could convey a resistance to checkpoint inhibition; however, so far no clinical data confirm this hypothesis. A better understanding on the regulatory factors of the immune system and tumor microenvironment is vital. Additional characterization of the composition and biological functions of immune infiltrates and their association with mutational tumor burden could constitute an important approach to select patients more likely to benefit from immunotherapy including immune checkpoint inhibition.

ACKNOWLEDGMENTS

We gratefully acknowledge the excellent laboratory work done by technicians Helle Wohlleben and Lone Christiansen. Parts of this study were based on data generated by the TCGA Research Network, and we thankfully acknowledge all tissue donors and workers involved in this project. This work was supported by grants from Danish Council for Independent Research (4183-00183), Fabrikant Einar Willumsens Mindefond, Familien Erichsens Mindefond, Købmand M. Kristjan Kjær og Hustru Margrethe Kjær, Født la Cour-Holmes Fond, Oda og Hans Svenningsens Fond, Thora og Viggo Groves Mindelegat, Harboefonden, A.J. Andersen og Hustrus Fond, Torben og Alice Frimodts Fond, Marie og Børge Kroghs Fond, and Arkitekt Holger Hjortenberg og Hustru Dagmar Hjortenbergs Fond.

ETHICS APPROVAL AND CONSENT TO PARTICIPATE

The study was approved by the Institutional Review Board of the Medical Faculty, Heinrich Heine University, Düsseldorf, Germany (Study No.5848R), the official Danish ethical review board named the Regional Scientific Ethical Committee of the Region of Southern Denmark (Project-ID: S-20150148), and the official Danish data registration authority (the Data Protection Authority, file number: 16/11065). The study was completed in agreement with the Declaration of Helsinki. The use of tissue was allowed by all patients in the Danish Tissue Application Register.

CONFLICT OF INTEREST

All authors declare that they have no conflicts of interest.

AUTHOR CONTRIBUTIONS

MDS and BWK conceived the study. MDS and ON designed the experiments. MDS and GR collected the data. MDS assembled the data and analyzed and interpreted the results. GR and BWK contributed with the reagents/materials/analysis tools. MDS drafted and edited the manuscript. All authors have read and approved the final manuscript.

DATA AVAILABILITY STATEMENT

The data that support the findings of this study are available from the corresponding author upon reasonable request.

REFERENCES

1. Hartmann C, Meyer J, Balss J, Capper D, Mueller W, Christians A, et al. Type and frequency of IDH1 and IDH2 mutations are related to astrocytic and oligodendroglial differentiation and age: a study of 1,010 diffuse gliomas. Acta Neuropathol. 2009;118:469–74.
2. Parsons DW, Jones S, Zhang X, Lin JC, Leary RJ, Angenendt P, et al. An integrated genomic analysis of human glioblastoma multiforme. Science. 2008;321:1807–12.
3. Yan H, Parsons DW, Jin G, McLendon R, Rasheed BA, Yuan W, et al. IDH1 and IDH2 mutations in gliomas. N Eng J Med. 2009;360:765–73.
4. Zhang C, Moore LM, Li X, Yung WK, Zhang W. IDH1/2 mutations target a key hallmark of cancer by deregulating cellular metabolism in glioma. Neuro-Oncology. 2013;15:1114–26.
5. Cairns RA, Mak TW. Oncogenic isocitrate dehydrogenase mutations: mechanisms, models, and clinical opportunities. Cancer Discov. 2013;3:730–41.
6. Horbinski C. What do we know about IDH1/2 mutations so far, and how do we use it? Acta Neuropathol. 2013;125:621–36.
7. Waitkus MS, Diplas BH, Yan H. Isocitrate dehydrogenase mutations in gliomas. Neuro-Oncology. 2016;18:16–26.
8. Mardis ER, Ding L, Dooling DJ, Larson DE, McLellan MD, Chen K, et al. Recurring mutations found by sequencing an acute myeloid leukemia genome. N Eng J Med. 2009;361:1058–66.
9. Tang JY, Chang CC, Lin PC, Chang JG. Isocitrate dehydrogenase mutation hot spots in acute lymphoblastic leukemia and oral cancer. Kaohsiung J Med Sci. 2012;28:138–44.
10. Cairns RA, Iqbal J, Lemonnier F, Kucuk C, de Leval L, Jais JP, et al. IDH2 mutations are frequent in angioimmunoblastic T-cell lymphoma. Blood. 2012;119:1901–3.
11. Amary MF, Bacsi K, Maggiani F, Damato S, Halai D, Berisha F, et al. IDH1 and IDH2 mutations are frequent events in central chondrosarcoma and central and periosteal chondromas but not in other mesenchymal tumours. J Pathol. 2011;224:334–43.
12. Damato S, Alorjani M, Bonar F, McCarthy SW, Cannon SR, O'Donnell P, et al. IDH1 mutations are not found in cartilaginous tumours other than central and periosteal chondrosarcomas and enchondromas. Histopathology. 2012;60:363–5.
13. Lopez GY, Reitman ZJ, Solomon D, Waldman T, Bigner DD, McLendon RE, et al. IDH1(R132) mutation identified in one human melanoma metastasis, but not correlated with metastases to the brain. Biochem Biophys Res Commun. 2010;398:585–7.
14. Borger DR, Tanabe KK, Fan KC, Lopez HU, Fantin VR, Straley KS, et al. Frequent mutation of isocitrate dehydrogenase (IDH)1 and IDH2 in cholangiocarcinoma identified through broad-based tumor genotyping. Oncologist. 2012;17:72–9.
15. Wang P, Dong Q, Zhang C, Kuan PF, Liu Y, Jeck WR, et al. Mutations in isocitrate dehydrogenase 1 and 2 occur frequently in intrahepatic cholangiocarcinomas and share hypermethylation targets with glioblastomas. Oncogene. 2013;32:3091–100.
16. Ghiam AF, Cairns RA, Thoms J, Dal Pra A, Ahmed O, Meng A, et al. IDH mutation status in prostate cancer. Oncogene. 2012;31:3826.
17. Bleeker FE, Atai NA, Lamba S, Jonker A, Rijkeboer D, Bosch KS, et al. The prognostic IDH1(R132) mutation is associated with reduced NADP+-dependent IDH activity in glioblastoma. Acta Neuropathol. 2010;119:487–94.
18. Dang L, White DW, Gross S, Bennett BD, Bittinger MA, Driggers EM, et al. Cancer-associated IDH1 mutations produce 2-hydroxyglutarate. Nature. 2009;462:739–44.
19. Jin G, Reitman ZJ, Spasojevic I, Batinic-Haberle I, Yang J, Schmidt-Kittler O, et al. 2-hydroxyglutarate production, but not dominant negative function, is conferred by glioma-derived NADP-dependent isocitrate dehydrogenase mutations. PLoS One. 2011;6:e16812.
20. Luoto S, Hermelo I, Vuorinen EM, Hannus P, Kesseli J, Nykter M, et al. Computational characterization of suppressive immune microenvironments in glioblastoma. Cancer Res. 2018;78:5574–85.
21. Turcan S, Rohle D, Goenka A, Walsh LA, Fang F, Yilmaz E, et al. IDH1 mutation is sufficient to establish the glioma hypermethylator phenotype. Nature. 2012;483:479–83.
22. Unruh D, Zewde M, Buss A, Drumm MR, Tran AN, Scholtens DM, et al. Methylation and transcription patterns are distinct in IDH mutant gliomas compared to other IDH mutant cancers. Sci Rep. 2019;9:8946.
23. Yang M, Soga T, Pollard PJ. Oncometabolites: linking altered metabolism with cancer. J Clin Invest. 2013;123:3652–8.
24. Unruh D, Mirkov S, Wray B, Drumm M, Lamano J, Li YD, et al. Methylation-dependent tissue factor suppression contributes to the reduced malignancy of IDH1-mutant gliomas. Clin Cancer Res. 2019;25:747–59.
25. Unruh D, Schwarze SR, Khoury L, Thomas C, Wu M, Chen L, et al. Mutant IDH1 and thrombosis in gliomas. Acta Neuropathol. 2016;132:917–30.
26. Zhang L, He L, Lugano R, Roodakker K, Bergqvist M, Smits A, et al. IDH mutation status is associated with distinct vascular gene expression signatures in lower-grade gliomas. Neuro-Oncology. 2018;20:1505–16.
27. Tomaszewski W, Sanchez-Perez L, Gajewski TF, Sampson JH. Brain tumor microenvironment and host state: implications for immunotherapy. Clin Cancer Res. 2019;25:4202–10.
28. Thorsson V, Gibbs DL, Brown SD, Wolf D, Bortone DS, Ou Yang TH, et al. The immune landscape of cancer. Immunity. 2018;48:812–30.e14.
29. Binnewies M, Roberts EW, Kersten K, Chan V, Fearon DF, Merad M, et al. Understanding the tumor immune microenvironment (TIME) for effective therapy. Nat Med. 2018;24:541–50.
30. Hodges TR, Ott M, Xiu J, Gatalica Z, Swensen J, Zhou S, et al. Mutational burden, immune checkpoint expression, and mismatch repair in glioma: implications for immune checkpoint immunotherapy. Neuro-Oncology. 2017;19:1047–57.
31. Amankulor NM, Kim Y, Arora S, Kargl J, Szulzewsky F, Hanke M, et al. Mutant IDH1 regulates the tumor-associated immune system in gliomas. Genes Dev. 2017;31:774–86.
32. Berghoff AS, Kiesel B, Widhalm G, Wilhelm D, Rajky O, Kurscheid S, et al. Correlation of immune phenotype with IDH mutation in diffuse glioma. Neuro-Oncology. 2017;19:1460–8
33. Bunse L, Pusch S, Bunse T, Sahm F, Sanghvi K, Friedrich M, et al. Suppression of antitumor T cell immunity by the oncometabolite (R)-2-hydroxyglutarate. Nature Med. 2018;24:1192–203.
34. Gao Y, Weenink B, van den Bent MJ, Erdem-Eraslan L, Kros JM, Sillevis Smitt P, et al. Expression-based intrinsic glioma subtypes are prognostic in low-grade gliomas of the EORTC22033-26033 clinical trial. Eur J Cancer. 2018;94:168–78.
35. Kohanbash G, Carrera DA, Shrivastav S, Ahn BJ, Jahan N, Mazor T, et al. Isocitrate dehydrogenase mutations suppress STAT1 and CD8+ T cell accumulation in gliomas. J Clin Invest. 2017;127:1425–37.
36. Poon CC, Gordon PMK, Liu K, Yang R, Sarkar S, Mirzaei R, et al. Differential microglia and macrophage profiles in human IDH-mutant and -wild type glioblastoma. Oncotarget. 2019;10:3129–43.
37. Zhang L, Sorensen MD, Kristensen BW, Reifenberger G, McIntyre TM, Lin F. D-2-Hydroxyglutarate is an intercellular mediator in IDH-mutant gliomas inhibiting complement and T cells. Clin Cancer Res. 2018;24:5381–91.
38. Liu PS, Wang H, Li X, Chao T, Teav T, Christen S, et al. Alpha-ketoglutarate orchestrates macrophage activation through metabolic and epigenetic reprogramming. Nat Immunol. 2017;18:985–94.

39. Liu S, Zhang C, Maimela NR, Yang L, Zhang Z, Ping Y, et al. Molecular and clinical characterization of CD163 expression via large-scale analysis in glioma. Oncoimmunology. 2019;8:e1601478.
40. Yuan Y, Zhao Q, Zhao S, Zhang P, Zhao H, Li Z, et al. Characterization of transcriptome profile and clinical features of a novel immunotherapy target CD204 in diffuse glioma. Cancer Med. 2019;8:3811–21.
41. Zhang X, Rao A, Sette P, Deibert C, Pomerantz A, Kim WJ, et al. IDH mutant gliomas escape natural killer cell immune surveillance by downregulation of NKG2D ligand expression. Neuro-Oncology. 2016;18:1402–12.
42. Mu L, Long Y, Yang C, Jin L, Tao H, Ge H, et al. The IDH1 mutation-induced oncometabolite, 2-hydroxyglutarate, may affect DNA methylation and expression of PD-L1 in gliomas. Front Mol Neurosci. 2018;11:82.
43. Wang Z, Wang Z, Zhang C, Liu X, Li G, Liu S, et al. Genetic and clinical characterization of B7–H3 (CD276) expression and epigenetic regulation in diffuse brain glioma. Cancer Sci. 2018;109:2697–705.
44. Zhang C, Zhang Z, Li F, Shen Z, Qiao Y, Li L, et al. Large-scale analysis reveals the specific clinical and immune features of B7–H3 in glioma. Oncoimmunology. 2018;7:e1461304.
45. Baumeister SH, Freeman GJ, Dranoff G, Sharpe AH. Coinhibitory pathways in immunotherapy for cancer. Ann Rev Immunol. 2016;34:539–73.
46. Koyama S, Akbay EA, Li YY, Herter-Sprie GS, Buczkowski KA, Richards WG, et al. Adaptive resistance to therapeutic PD-1 blockade is associated with upregulation of alternative immune checkpoints. Nat Commun. 2016;7:10501.
47. Qin S, Xu L, Yi M, Yu S, Wu K, Luo S. Novel immune checkpoint targets: moving beyond PD-1 and CTLA-4. Mol Cancer. 2019;18:155.
48. Du W, Yang M, Turner A, Xu C, Ferris RL, Huang J, et al. TIM-3 as a target for cancer immunotherapy and mechanisms of action. Int J Mol Sci. 2017;18:645.
49. Goods BA, Hernandez AL, Lowther DE, Lucca LE, Lerner BA, Gunel M, et al. Functional differences between PD-1+ and PD-1- CD4+ effector T cells in healthy donors and patients with glioblastoma multiforme. PLoS One. 2017;12:e0181538.
50. Lowther DE, Goods BA, Lucca LE, Lerner BA, Raddassi K, van Dijk D, et al. PD-1 marks dysfunctional regulatory T cells in malignant gliomas. JCI Insight. 2016;1:e85935.
51. Sakuishi K, Apetoh L, Sullivan JM, Blazar BR, Kuchroo VK, Anderson AC. Targeting Tim-3 and PD-1 pathways to reverse T cell exhaustion and restore anti-tumor immunity. J Exp Med. 2010;207:2187–94.
52. Ocana-Guzman R, Torre-Bouscoulet L, Sada-Ovalle I. TIM-3 regulates distinct functions in macrophages. Front Immunol. 2016;7:229.
53. Yan W, Liu X, Ma H, Zhang H, Song X, Gao L, et al. Tim-3 fosters HCC development by enhancing TGF-beta-mediated alternative activation of macrophages. Gut. 2015;64:1593–604.
54. Yang X, Jiang X, Chen G, Xiao Y, Geng S, Kang C, et al. T cell Ig Mucin-3 promotes homeostasis of sepsis by negatively regulating the TLR response. J Immunol. 2013;190:2068–79.
55. Liang T, Wang X, Wang F, Feng E, You G. Galectin-9: a predictive biomarker negatively regulating immune response in glioma patients. World Neurosurg. 2019;9:e455–e462.
56. Liu Z, Han H, He X, Li S, Wu C, Yu C, et al. Expression of the galectin-9-Tim-3 pathway in glioma tissues is associated with the clinical manifestations of glioma. Oncol Lett. 2016;11:1829–34.
57. Yuan F, Ming H, Wang Y, Yang Y, Yi L, Li T, et al. Molecular and clinical characterization of Galectin-9 in glioma through 1,027 samples. J Cell Physiol. 2019;235:4326–34.
58. Li G, Wang Z, Zhang C, Liu X, Cai J, Wang Z, et al. Molecular and clinical characterization of TIM-3 in glioma through 1,024 samples. Oncoimmunology. 2017;6:e1328339.
59. Li X, Wang B, Gu L, Zhang J, Li X, Gao L, et al. Tim-3 expression predicts the abnormal innate immune status and poor prognosis of glioma patients. Clin Chim Acta. 2018;476:178–84.
60. Ligon KL, Alberta JA, Kho AT, Weiss J, Kwaan MR, Nutt CL, et al. The oligodendroglial lineage marker OLIG2 is universally expressed in diffuse gliomas. J Neuropathol Exp Neurol. 2004;63:499–509.
61. Popova SN, Bergqvist M, Dimberg A, Edqvist PH, Ekman S, Hesselager G, et al. Subtyping of gliomas of various WHO grades by the application of immunohistochemistry. Histopathology. 2014;64:365–79.
62. Louis DN, Ohgaki H, Wiestler OD, Cavenee WK, Ellison DW, Figarella-Branger D, et al. WHO classification of tumours of the central nervous system, Revised. 4th ed. Lyon: International Agency for Research on Cancer (IARC); 2016.
63. Dahlrot RH, Kristensen BW, Hjelmborg J, Herrstedt J, Hansen S. A population-based study of low-grade gliomas and mutated isocitrate dehydrogenase 1 (IDH1). J Neuro-Oncol. 2013;114:309–17.
64. Petterson SA, Sørensen MD, Kristensen BW. Expression profiling of primary and recurrent glioblastomas reveals a reduced level of pentraxin 3 in recurrent glioblastomas. J Neuropathol Exp Neurol. 2020;79:975–85.
65. Sorensen MD, Dahlrot RH, Boldt HB, Hansen S, Kristensen BW. Tumour-associated microglia/macrophages predict poor prognosis in high-grade gliomas and correlate with an aggressive tumour subtype. Neuropathol Appl Neurobiol. 2018;44:185–206.
66. Bowman RL, Wang Q, Carro A, Verhaak RG, Squatrito M. GlioVis data portal for visualization and analysis of brain tumor expression datasets. Neuro-Oncology. 2017;19:139–41.
67. Ceccarelli M, Barthel FP, Malta TM, Sabedot TS, Salama SR, Murray BA, et al. Molecular profiling reveals biologically discrete subsets and pathways of progression in diffuse glioma. Cell. 2016;164:550–63.
68. The Cancer Genome Atlas Research Network. Comprehensive genomic characterization defines human glioblastoma genes and core pathways. Nature. 2008;455:1061–8.
69. Hao N-B, Lü M-H, Fan Y-H, Cao Y-L, Zhang Z-R, Yang S-M. Macrophages in tumor microenvironments and the progression of tumors. Clin Dev Immunol. 2012;2012:948098.
70. Li W, Graeber MB. The molecular profile of microglia under the influence of glioma. Neuro-Oncology. 2012;14:958–78.
71. Mantovani A, Sica A, Sozzani S, Allavena P, Vecchi A, Locati M. The chemokine system in diverse forms of macrophage activation and polarization. Trends Immunol. 2004;25:677–86.
72. Rabenstein M, Vay SU, Flitsch LJ, Fink GR, Schroeter M, Rueger MA. Osteopontin directly modulates cytokine expression of primary microglia and increases their survival. J Neuroimmunol. 2016;299:130–8.
73. Szulzewsky F, Pelz A, Feng X, Synowitz M, Markovic D, Langmann T, et al. Glioma-associated microglia/macrophages display an expression profile different from M1 and M2 polarization and highly express Gpnmb and Spp1. PLoS One. 2015;10: e0116644.
74. Monney L, Sabatos CA, Gaglia JL, Ryu A, Waldner H, Chernova T, et al. Th1-specific cell surface protein Tim-3 regulates macrophage activation and severity of an autoimmune disease. Nature. 2002;415:536–41.
75. Velasquez C, Mansouri S, Mora C, Nassiri F, Suppiah S, Martino J, et al. Molecular and clinical insights into the invasive capacity of glioblastoma cells. J Oncol. 2019;2019:1740763.
76. Cai J, Zhang W, Yang P, Wang Y, Li M, Zhang C, et al. Identification of a 6-cytokine prognostic signature in patients with primary glioblastoma harboring M2 microglia/macrophage phenotype relevance. PLoS One. 2015;10:e0126022.
77. Deng S, Zhu S, Qiao Y, Liu YJ, Chen W, Zhao G, et al. Recent advances in the role of toll-like receptors and TLR agonists in immunotherapy for human glioma. Protein Cell. 2014;5:899–911.

78. Liang H, Yi L, Wang X, Zhou C, Xu L. Interleukin-17 facilitates the immune suppressor capacity of high-grade glioma-derived CD4 (+) CD25 (+) Foxp3 (+) T cells via releasing transforming growth factor beta. Scand J Immunol. 2014;80:144–50.
79. Parajuli P, Mittal S. Role of IL-17 in glioma progression. J Spine Neurosurg. 2013;(Suppl 1). https://doi.org/10.4172/2325-9701.S1-004.
80. Zhang Y, Cai P, Liang T, Wang L, Hu L. TIM-3 is a potential prognostic marker for patients with solid tumors: a systematic review and meta-analysis. Oncotarget. 2017;8:31705–13.
81. Venteicher AS, Tirosh I, Hebert C, Yizhak K, Neftel C, Filbin MG, et al. Decoupling genetics, lineages, and microenvironment in IDH-mutant gliomas by single-cell RNA-seq. Science. 2017;355:eaai8478.
82. Phillips HS, Kharbanda S, Chen R, Forrest WF, Soriano RH, Wu TD, et al. Molecular subclasses of high-grade glioma predict prognosis, delineate a pattern of disease progression, and resemble stages in neurogenesis. Cancer Cell. 2006;9:157–73.
83. Verhaak RGW, Hoadley KA, Purdom E, Wang V, Qi Y, Wilkerson MD, et al. An integrated genomic analysis identifies clinically relevant subtypes of glioblastoma characterized by abnormalities in PDGFRA, IDH1, EGFR and NF1. Cancer Cell. 2010;17:98–110.
84. Noushmehr H, Weisenberger DJ, Diefes K, Phillips HS, Pujara K, Berman BP, et al. Identification of a CpG island methylator phenotype that defines a distinct subgroup of glioma. Cancer Cell. 2010;17:510–22.
85. Helmy K, Halliday J, Fomchenko E, Setty M, Pitter K, Hafemeister C, et al. Identification of global alteration of translational regulation in glioma in vivo. PLoS One. 2012;7:e46965.
86. Vogel C, Marcotte EM. Insights into the regulation of protein abundance from proteomic and transcriptomic analyses. Nat Rev Genet. 2012;13:227–32.
87. Ilie M, Beaulande M, Ben Hadj S, Chamorey E, Schiappa R, Long-Mira E, et al. Chromogenic multiplex immunohistochemistry reveals modulation of the immune microenvironment associated with survival in elderly patients with lung adenocarcinoma. Cancers. 2018;10:326.
88. Ilie M, Beaulande M, Hamila M, Erb G, Hofman V, Hofman P. Automated chromogenic multiplexed immunohistochemistry assay for diagnosis and predictive biomarker testing in non-small cell lung cancer. Lung Cancer. 2018;124:90–4.
89. Rakaee M, Busund L-TR, Jamaly S, Paulsen E-E, Richardsen E, Andersen S, et al. Prognostic value of macrophage phenotypes in resectable non-small cell lung cancer assessed by multiplex immunohistochemistry. Neoplasia. 2019;21:282–93.
90. Stack EC, Wang C, Roman KA, Hoyt CC. Multiplexed immunohistochemistry, imaging, and quantitation: a review, with an assessment of Tyramide signal amplification, multispectral imaging and multiplex analysis. Methods. 2014;70:46–58.
91. Giraldo NA, Nguyen P, Engle EL, Kaunitz GJ, Cottrell TR, Berry S, et al. Multidimensional, quantitative assessment of PD-1/PD-L1 expression in patients with Merkel cell carcinoma and association with response to pembrolizumab. J Immunother Cancer. 2018;6:99.
92. Saylor J, Ma Z, Goodridge HS, Huang F, Cress AE, Pandol SJ, et al. Spatial mapping of myeloid cells and macrophages by multiplexed tissue staining. Front Immunol. 2018;9:2925.
93. Hirashima M, Kashio Y, Nishi N, Yamauchi A, Imaizumi TA, Kageshita T, et al. Galectin-9 in physiological and pathological conditions. Glycoconj J. 2002;19:593–600.
94. John S, Mishra R. Galectin-9: From cell biology to complex disease dynamics. J Biosci. 2016;41:507–34.
95. Steelman AJ, Li J. Astrocyte galectin-9 potentiates microglial TNF secretion. J Neuroinflammation. 2014;11:144.
96. Steelman AJ, Smith R 3rd, Welsh CJ, Li J. Galectin-9 protein is up-regulated in astrocytes by tumor necrosis factor and promotes encephalitogenic T-cell apoptosis. J Biol Chem. 2013;288:23776–87.
97. Thijssen VL, Hulsmans S, Griffioen AW. The galectin profile of the endothelium: altered expression and localization in activated and tumor endothelial cells. Am J Pathol. 2008;172:545–53.
98. Kim Y, Park J, Choi YK. The role of astrocytes in the central nervous system focused on bk channel and heme oxygenase metabolites: a review. Antioxidants (Basel). 2019;8:121.
99. Han S, Feng S, Xu L, Shi W, Wang X, Wang H, et al. Tim-3 on peripheral CD4(+) and CD8(+) T cells is involved in the development of glioma. DNA Cell Biol. 2014;33:245–50.
100. Han S, Ma E, Wang X, Yu C, Dong T, Zhan W, et al. Rescuing defective tumor-infiltrating T-cell proliferation in glioblastoma patients. Oncol Lett. 2016;12:2924–9.
101. Mohme M, Schliffke S, Maire CL, Runger A, Glau L, Mende KC, et al. Immunophenotyping of newly diagnosed and recurrent glioblastoma defines distinct immune exhaustion profiles in peripheral and tumor-infiltrating lymphocytes. Clin Cancer Res. 2018;24:4187–200.
102. Kim JE, Patel MA, Mangraviti A, Kim ES, Theodros D, Velarde E, et al. Combination therapy with anti-PD-1, anti-TIM-3, and focal radiation results in regression of murine gliomas. Clin Cancer Res. 2017;23:124–36.
103. Goncalves Silva I, Yasinska IM, Sakhnevych SS, Fiedler W, Wellbrock J, Bardelli M, et al. The Tim-3-galectin-9 secretory pathway is involved in the immune escape of human acute myeloid leukemia cells. EBioMedicine. 2017;22:44–57.
104. Kikushige Y, Miyamoto T, Yuda J, Jabbarzadeh-Tabrizi S, Shima T, Takayanagi S-i, et al. A TIM-3/Gal-9 autocrine stimulatory loop drives self-renewal of human myeloid leukemia stem cells and leukemic progression. Cell Stem Cell. 2015;17:341–52.
105. Yasinska IM, Sakhnevych SS, Pavlova L, Teo Hansen Selno A, Teuscher Abeleira AM, Benlaouer O, et al. The Tim-3-Galectin-9 pathway and its regulatory mechanisms in human breast cancer. Front Immunol. 2019;10:1594.
106. Ma CJ, Li GY, Cheng YQ, Wang JM, Ying RS, Shi L, et al. Cis association of Galectin-9 with Tim-3 differentially regulates IL-12/IL-23 expressions in monocytes via TLR signaling. PLoS One. 2013;8:e72488.
107. Charoentong P, Finotello F, Angelova M, Mayer C, Efremova M, Rieder D, et al. Pan-cancer immunogenomic analyses reveal genotype-immunophenotype relationships and predictors of response to checkpoint blockade. Cell Rep. 2017;18:248–62.

SUPPORTING INFORMATION

Additional supporting information may be found online in the Supporting Information section.

FIGURE S1 Co-expression patterns of Gal-9 and TIM-3 in IDH1 R132H-mutant WHO III-IV astrocytic gliomas. IDH1 R132-mutant glial tumor cells rarely expressed Gal-9 (A,B) and TIM-3 (C,D). *Scale bar* 100 μM

FIGURE S2 Correlation analyses in WHO grade III and IV astrocytic gliomas. (A,B) A positive correlation was found between total Gal-9 cell count (in %) and total TIM-3 cell count (in %) in the astrocytoma cohort used for the multiplex chromogenic immunohistochemistry study. Additionally, positive correlations were found among Gal-9, TIM-3 and T cell markers CD4, CD8, and FOXP3, while OLIG2 was negatively correlated with Gal-9, TIM-3 as well as CD4 and CD8. (C,D) *Gal-9* mRNA expression was positively correlated with *TIM-3* mRNA levels in the TCGA dataset. Both *TIM-3*

and *Gal-9* showed a moderate-strong correlation with mRNA levels of the T cell markers *CD4*, *CD8A*/*B* and *FOXP3*, while *OLIG2* mRNA levels were negatively correlated with *TIM-3*, *Gal-9* and the T cell markers to a weak-moderate degree

FIGURE S3 Association between glioma subtype and mRNA expression levels in the TCGA dataset. (A,B) OD had the lowest *Gal-9* (A) and *TIM-3* (B) mRNA expression level compared to other five glioma subtypes, while GBM, WHO grade IV, and IDH-wildtype diffuse and anaplastic astrocytomas, WHO grade II and III, appeared to have the highest expression levels. (C) OD and AOD had the lowest mRNA expression level of *CD4* compared to the four astrocytic subtypes. Further, IDH-wildtype GBM had higher *CD4* levels than IDH-mutant astrocytomas of WHO grades II and III. (D,E) *CD8A* and *CD8B* mRNA expression levels were lower in oligodendroglial tumors and IDH-mutant astrocytomas compared IDH-wildtype astrocytomas. (F) Oligodendroglial tumors and IDH-wildtype astrocytoma, WHO grade II- III and IV, had the highest mRNA expression level of *FOXP3*. *Horizontal lines* indicate mean (A,C,D) or median (B,E,F). *Vertical lines* indicate ± standard error of the mean (SEM) (A,C,D). *$p < 0.05$; **$p < 0.01$; ***$p < 0.001$. AA, anaplastic astrocytoma; AOD, anaplastic oligodendroglioma; DA, diffuse astrocytoma; GBM, glioblastoma; IDH, isocitrate dehydrogenase; mIDH, IDH-mutant; OD, oligodendroglioma; wtIDH, IDH-wildtype

FIGURE S4 *IBA-1* mRNA expression in the TCGA dataset. (**A**) OD and AOD had lower IBA-1 mRNA expression level compared to the four astrocytic tumor groups, while no differences in mRNA levels were observed among the astrocytic groups. (B,C) *IBA-1* mRNA expression levels were positively correlated to mRNA expression of Gal-9 (B) and TIM-3 (C). *Horizontal* and *vertical lines* indicate mean and ± standard error of the mean (SEM), respectively. ***$p < 0.001$. AA, anaplastic astrocytoma; AOD, anaplastic oligodendroglioma; DA, diffuse astrocytoma; GBM, glioblastoma; IDH, isocitrate dehydrogenase; mIDH, IDH-mutant; OD, oligodendroglioma; wtIDH, IDH-wildtype

FIGURE S5 Expression levels of microglia/macrophage-related markers in IDH-mutant *vs*. IDH-wildtype astrocytic gliomas of WHO grade III and IV. (A,B) Expression of mRNA *IBA-1* and protein IBA-1 did not differ between IDH-mutant and IDH-wildtype tumors. (C,D). In contrast, expression of the M2-related CD204 was significantly lower in IDH-mutant tumors at both the mRNA and the protein levels. (E-G) mRNA levels of the M2-related markers *IL6* (E), *TLR1* (F), and *TLR8* (G) were decreased in IDH-mutant tumors compared to IDH-wildtype tumors. (H-K) mRNA expression of the M1-related markers *IL1B* (H), *IL18* (I), *TLR2* (J), and *CCL2* (K) was diminished in IDH-mutant tumors compared to IDH-wildtype tumors. (L) *SPP1* mRNA levels were significantly lower in IDH-mutant tumors. *Horizontal lines* indicate the mean (A,C,F,G,I-L) or the median (B,D,E,H). *Vertical lines* indicate ± standard error of the mean (SEM). AA, anaplastic astrocytoma; AOD, anaplastic oligodendroglioma; DA, diffuse astrocytoma; GBM, glioblastoma; IDH, isocitrate dehydrogenase; mIDH, IDH-mutant; OD, oligodendroglioma; wtIDH, IDH-wildtype

TABLE S1 Antibodies and detection systems used for double immunofluorescence

TABLE S2 Differentially upregulated genes in TIM-3 enriched glioblastomas in the TCGA dataset

TABLE S3 KEGG enrichment analysis

TABLE S4 Gene Ontology enrichment analysis (biological processes)

How to cite this article: D. Sørensen M, Nielsen O, Reifenberger G, W. Kristensen B. The presence of TIM-3 positive cells in WHO grade III and IV astrocytic gliomas correlates with isocitrate dehydrogenase mutation status. *Brain Pathology*. 2021;31:e12921. https://doi.org/10.1111/bpa.12921